

Anomaly Resilient Temporal QoS Prediction using Hypergraph Convoluted Transformer Network

Suraj Kumar, Soumi Chattopadhyay, *Senior Member, IEEE*, Chandranath Adak, *Senior Member, IEEE*

Abstract—Quality-of-Service (QoS) prediction is a critical task in the service lifecycle, enabling precise and adaptive service recommendations by anticipating performance variations over time in response to evolving network uncertainties and user preferences. However, contemporary QoS prediction methods frequently encounter data sparsity and cold-start issues, which hinder accurate QoS predictions and limit the ability to capture diverse user preferences. Additionally, these methods often assume QoS data reliability, neglecting potential credibility issues such as outliers and the presence of greysheep users and services with atypical invocation patterns. Furthermore, traditional approaches fail to leverage diverse features, including domain-specific knowledge and complex higher-order patterns, essential for accurate QoS predictions. In this paper, we introduce a real-time, trust-aware framework for temporal QoS prediction to address the aforementioned challenges, featuring an end-to-end deep architecture called the Hypergraph Convoluted Transformer Network (HCTN). HCTN combines a hypergraph structure with graph convolution over hyper-edges to effectively address high-sparsity issues by capturing complex, high-order correlations. Complementing this, the transformer network utilizes multi-head attention along with parallel 1D convolutional layers and fully connected dense blocks to capture both fine-grained and coarse-grained dynamic patterns. Additionally, our approach includes a sparsity-resilient solution for detecting greysheep users and services, incorporating their unique characteristics to improve prediction accuracy. Trained with a robust loss function resistant to outliers, HCTN demonstrated state-of-the-art performance on the large-scale WSDREAM-2 datasets for response time and throughput.

Index Terms—Graph convolution, Hypergraph, Temporal QoS prediction, Transformer network

I. INTRODUCTION

Over the past decade, service-oriented architectures (SOA) [1] such as Google Cloud Platform and Amazon Web Services have revolutionized software development by speeding up application creation, reducing costs, and enhancing scalability. This evolution has led to the widespread use of web services for low-cost communication and has driven the Everything-as-a-Service paradigm [2], prompting businesses to adopt SOA across sectors such as food, healthcare, and transportation. However, with numerous similar services available, users often struggle to choose the best option, often relying on past

experiences or external opinions, a behavior known as the bandwagon effect [3]. The incomplete information about available options exacerbates this issue. Researchers emphasize the importance of non-functional parameters, collectively referred to as *Quality of Service* (QoS) [4]–[6], for distinguishing between services. QoS can vary due to factors like network conditions, invocation time, and contextual elements. Manually assessing the QoS of millions of services is impractical and costly, underscoring the need for QoS prediction tools to assist in service recommendation.

Researchers have addressed service selection through automatic QoS prediction, with Collaborative Filtering (CF) being a prominent method that identifies correlations between users and services [7], [8]. CF is divided into Memory-based and Model-based approaches. Memory-based CF estimates QoS by calculating similarities but suffers from high computational cost and data sparsity [4], [5], [9]. Model-based CF methods like Matrix Factorization (MF) [10], [11], Factorization Machines (FM) [12], and deep learning models [13]–[15] handle sparsity by learning latent features, with FM capturing second-order interactions and deep learning models addressing higher-order features. Hybrid models combine both to improve accuracy [15]. However, many assume static QoS parameters [11], [16], though QoS can fluctuate over time. While some methods model temporal QoS, they struggle with data anomalies, resulting in unreliable predictions [6], [13], [17], [18].

We identify three key factors causing accuracy degradation in temporal QoS prediction: (a) *Data Deficiency*: Sparse QoS experiences, especially in cold-start scenarios, arise from limited user-service interactions [19]. (b) *Data Credibility*: Dynamic environments introduce outliers, while the greysheep problem complicates predictions for atypical instances with unique traits. (c) *Data Learning*: Traditional methods using similarity features [4], [5] or linear matrix decomposition [10], [11] fail to capture complex user-service relationships over time. While some approaches leverage Graph Convolutional Networks (GCNs) [19], [20] enhance feature learning, they struggle with temporal dynamics, and models like ARIMA [21], Recurrent Neural Networks [13], [22], and Transformer networks [18] enhance temporal feature learning, they often overlook local spatial context and struggle with data anomalies, impacting accuracy. A recent study, TPMCF [18], employs distinct architectures to separately capture spatial and temporal features but faces challenges in managing certain data anomalies, which impacts its prediction accuracy.

Considering the abovementioned extremity, we propose an anomaly-resilient temporal QoS prediction framework called

Suraj Kumar and Soumi Chattopadhyay are with the Dept. of CSE, Indian Institute of Technology Indore, Madhya Pradesh 452020, India. (email: {phd2301101002, soumi}@iiti.ac.in).

Chandranath Adak is with the Dept. of CSE, Indian Institute of Technology Patna, Bihar 801106, India. (e-mail: chandranath@iitp.ac.in). Corresponding author: Soumi Chattopadhyay.

This work has been submitted to the IEEE for possible publication. Copyright may be transferred without notice, after which this version may no longer be accessible.

Hypergraph Convolved Transformer Network (HCTN), an end-to-end architecture with five key components: (a) The first module applies non-negative matrix decomposition to extract latent user and service features, addressing data sparsity and cold-start issues. (b) The second module uses hypergraph collaborative filtering to capture high-order user-service features through hypergraph convolution over hyperedges, further addressing sparsity. (c) To tackle the greysheep problem, the third module emphasizes local characteristics of greysheep users and services, enhancing the effectiveness of collaborative filtering. (d) The next module refines temporal granularity by feeding updated embeddings into an enhanced transformer network that combines multi-head attention [23] with parallel 1D-convolutional layers and fully connected networks. This enables the model to capture fine- and coarse-grained temporal patterns, providing a rich representation of both short-term variations and long-term trends. (e) The final module predicts QoS by integrating collaborative, spatial, and temporal features, with the entire model trained end-to-end using an outlier-resilient loss function to handle anomalies. This framework effectively addresses data sparsity, cold-start, greysheep, and temporal dynamics challenges, providing accurate QoS predictions. In summary, this paper has following **contributions**:

(i) *Novelty in model architecture*: We introduce the Hypergraph Convolved Transformer Network (HCTN) for temporal QoS prediction. HCTN combines hypergraph learning for higher-order collaborative filtering with dual-channel Transformer networks, capturing dynamic features from fine-to-coarse-grained levels and using multi-head attention to manage various contexts.

(ii) *Handling data deficiency*: We address data sparsity using higher-order collaborative filtering with diverse hyperedges in second-order user-service graphs. Additionally, non-negative matrix decomposition uncovers hidden user and service preferences, improving cold-start performance and enhancing collaborative filtering features.

(iii) *Tackling data credibility*: To address data credibility, we apply two sparsity-resilient unsupervised algorithms to detect outliers and greysheep. Outliers are handled with a logarithmic penalty on training errors, while greysheep are managed by prioritizing their unique patterns over global collaborative filtering features, improving QoS prediction.

(iv) *Rich data representation*: In our framework, domain knowledge features, such as latent user preferences and service characteristics, are combined with higher-order complex spatio-temporal features to effectively capture the intricate triadic relationships among users, services, and time, thereby enhancing overall data representation.

(v) *Extensive experiments*: We conducted comprehensive experiments using the QoS benchmark dataset, WSDREAM-2 [24], for two different QoS parameters, response time and throughput. These experiments highlight the superior performance of HCTN compared to contemporary methods. Additionally, our ablation study validates the effectiveness of each module within the proposed framework.

The remaining paper is organized as follows: Section II formulates the temporal QoS prediction problem. Section III details our framework. Section IV presents the experiments

and comparative studies. Section V reviews existing works. Finally, Section VI concludes the paper and outlines future research directions.

II. PROBLEM FORMULATION

In this section, we mathematically define the temporal QoS prediction problem. Consider a dynamic web-services ecosystem with n users, denoted as $\mathcal{U} = \{u_1, u_2, \dots, u_n\}$ and m services, denoted as $\mathcal{S} = \{s_1, s_2, \dots, s_m\}$. We monitor their interaction over the past \mathcal{T} time-steps through a QoS invocation tensor $\mathcal{Q}_{n \times m \times \mathcal{T}}$ in terms of a QoS parameter q . It may be noted that \mathcal{Q} is a sparse tensor where valid entries are positive real numbers, while zeros represent invalid entries. The objective of the classical temporal QoS prediction is to estimate the missing value of $\mathcal{Q}(i, j, t)$, which indicates the QoS value of service s_j for user u_i at time-step t .

The classical temporal QoS prediction problem often encounters three main research challenges, which can be categorized into six key research questions (RQ):

(i) **Data deficiency**: Insufficient QoS observations lead to high sparsity in \mathcal{Q} due to:

- *RQ1. Limited user-service interactions*: Users $u_i \in \mathcal{U}$ do not interact with all services $s_j \in \mathcal{S}$ at each time-step t , resulting in a sparse QoS vector $\mathcal{Q}^t(i, \cdot)$, where \mathcal{Q}^t represents the QoS invocation matrix recorded at t^{th} time-step. How can we effectively leverage this sparse data for reliable QoS predictions?

- *RQ2. Cold-start problem*: Newly added users or services have little to no interaction data. How can we effectively predict QoS for these new users or services despite the absence of historical data?

(ii) **Data credibility**: Unreliable QoS data can degrade prediction accuracy, driven by:

- *RQ3. Outliers problem*: Dynamic factors such as limited network bandwidth or competition among service providers can cause outliers in QoS data. How can we effectively suppress these outliers to ensure reliable QoS predictions?

- *RQ4. Greysheep problem*: Some users or services may exhibit a unique QoS invocation pattern that significantly deviates from others, termed as *greysheep*. How can we detect and leverage their characteristics for better predictions?

(iii) **Data representation problem**: The QoS invocation pattern of a user or service can vary due to various known and unknown factors. Thus, capturing the diverse characteristics of users and services is crucial for accurate feature representation and QoS prediction:

- *RQ5. Domain-specific features*: How can we effectively use domain-specific features, such as user preferences and service characteristics, to improve prediction stability, speed, and accuracy?

- *RQ6. Higher-order features*: In addition to domain knowledge features, it is crucial to explore complex, higher-order features such as spatial and temporal granularity for better data representation learning. How can we harness these intricate features for enhanced QoS prediction?

The objective of this paper is to introduce an anomaly-resilient temporal QoS prediction framework designed to address the aforementioned research questions.

III. PROPOSED METHOD

This section introduces our proposed framework for anomaly-resilient real-time temporal QoS prediction comprising an end-to-end Hypergraph Convolved Transformer Network (HCTN) that is composed of five primary modules: (a) *Global Pattern Adaptation Module (GPAM)*: This module exploits domain-specific global features using non-negative matrix decomposition, which also helps to alleviate the cold-start problem. (b) *Hypergraph Collaborative Filtering Module (HCFM)*: This module leverages a hypergraph convolution network to extract higher-order spatial collaborative features, effectively addressing the challenge of high data sparsity. (c) *Greysheep Mitigation Module (GMM)*: This module tackles the QoS prediction challenges posed by greysheep users and services. It includes two sub-modules: the Greysheep Detection Module (GDM), which identifies greysheep users and services, and the Local Pattern Adaptation Module (LPAM), which enriches these greysheep with additional local features to improve QoS prediction performance. (d) *Temporal Granularity Extraction Module (TGEM)*: This module captures fine-to-coarse-grained temporal features using multi-head attention, enhancing the learning of different data representations. (e) *Comprehensive QoS Prediction Module (CQPM)*: This final module of HCTN is responsible for predicting the missing QoS values.

By leveraging the diverse features obtained from various modules of HCTN, the overall goal of the framework is to deliver highly accurate real-time temporal QoS predictions while effectively addressing the challenges outlined in Section II. A brief overview of HCTN is presented in Fig. 2. We now illustrate each module of HCTN in detail.

A. Global Pattern Adaptation Module (GPAM)

The primary purpose of the GPAM is to provide domain-specific features by preserving the global characteristics of user-service interactions at a given time-step t . These features contribute to generating initial feature embeddings for each user and service. GPAM employs Non-negative Matrix Decomposition (NMD) [10] to uncover hidden QoS invocation patterns among users and services.

Given a QoS invocation matrix \mathcal{Q}^t for n users and m services, NMD decomposes \mathcal{Q}^t into two low-rank latent features matrices, \mathcal{X}_u^t and \mathcal{X}_s^t , such that:

$$\mathcal{Q}_{n \times m}^t(i, j) \approx [(\mathcal{X}_u^t)_{n \times f_1} \cdot (\mathcal{X}_s^t)_{m \times f_1}^T](i, j), \quad \forall \mathcal{Q}^t(i, j) \geq 0$$

By applying NMD to each of the previous τ time-steps, GPAM extracts f_1 -dimensional features for users and services, as depicted in Fig. 2(c). This process yields two feature tensors:

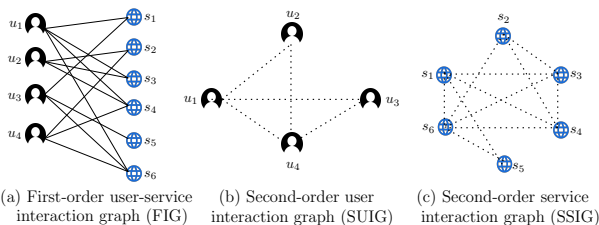


Fig. 1: Decomposition of QIHG: (a) FIG, (b) SUIG, (c) SSIG

\mathcal{X}_u with dimensions $n \times f_1 \times \tau$, and \mathcal{X}_s with dimensions $m \times f_1 \times \tau$, corresponding to users and services, respectively. These user and service features are further combined into a user-service feature tensor \mathcal{X}_0 with dimensions $N \times f_1 \times \tau$, where $N = n + m$, by row-wise concatenating each \mathcal{X}_u^t and \mathcal{X}_s^t . These feature embeddings are utilized in the next module discussed in Section III-B. Notably, GPAM produces dense feature tensors, which help mitigate the cold-start problem without requiring additional interventions.

B. Hypergraph Collaborative Filtering Module (HCFM)

GPAM effectively provides collaborative features that partially address the data-sparsity problem. However, it falls short in capturing higher-order, non-linear, and complex features of users and services that are essential for high prediction performance. To address this, various GCN-based frameworks [18]–[20], [25] have been introduced in the literature, utilizing bipartite graph representations of user-service QoS interactions. However, user-service interactions can extend beyond bipartite connections, leading to multidimensional relationships represented by hyper-edges. In this paper, we propose a Hypergraph Convolution Network (HCN), as presented in Fig. 2(b), to exploit these connections. HCN primarily leverages graph convolution over various graph representations constructed using different hyper-edges, as shown in Fig. 1. Before discussing the details of this module, we first introduce the concept of a hypergraph in the context of QoS invocation.

1) *Hypergraph to Represent QoS Invocation*: The connectivity between users and services to form a graph structure can be established through various methods, such as by shared autonomous systems or geographical locations. However, due to privacy concerns, we may not always have access to such details. To address this issue, we construct a hypergraph structure based on their past interactions recorded in the QoS invocation matrix at a given time-step t . For each time-step t , we define the QoS invocation hypergraph in Definition III.1.

Definition III.1. [QoS Invocation Hypergraph (QIHG)]: Given a set of users \mathcal{U} and services \mathcal{S} , the QoS Invocation Hypergraph (QIHG) at time-step t , denoted by \mathcal{G}^t , is defined as $\mathcal{G}^t = (\mathcal{V}_u \cup \mathcal{V}_s, \mathcal{E}^t)$. Here, \mathcal{V}_u represents the set of users \mathcal{U} , and \mathcal{V}_s represents the set of services \mathcal{S} . The hyperedges \mathcal{E}^t extend beyond simple pairwise connections and are of two types: (i) a hyperedge $\{v_i^u, v_j^s, v_k^u\}$, indicating that both users u_i and u_k corresponding to v_i^u and $v_k^u \in \mathcal{V}_u$ invoked service s_j corresponding to $v_j^s \in \mathcal{V}_s$ at time-step t ; and (ii) a hyperedge $\{v_i^s, v_j^u, v_k^s\}$, indicating that both services s_i and s_k corresponding to v_i^s and $v_k^s \in \mathcal{V}_s$ were invoked by user u_j corresponding to $v_j^u \in \mathcal{V}_u$ at time-step t . ■

We simplify the complex hypergraph \mathcal{G}^t by decomposing it into three distinct graphs, each capturing a specific type of relationship among users and services:

(a) *First-order user-service Interaction Graph (FIG)*: The FIG, denoted as $\mathcal{G}_f^t = (\mathcal{V}_u \cup \mathcal{V}_s, \mathcal{E}_f^t)$, captures direct interactions between users and services. An edge $(v_i^u, v_j^s) \in \mathcal{E}_f^t$ exists if the user corresponding to $v_i^u \in \mathcal{V}_u$ invoked the service corresponding to $v_j^s \in \mathcal{V}_s$ at time-step t . \mathcal{G}_f^t is represented by an adjacency matrix $\mathcal{A}^t \in \{0, 1\}_{N \times N}$, where $N = n + m$.

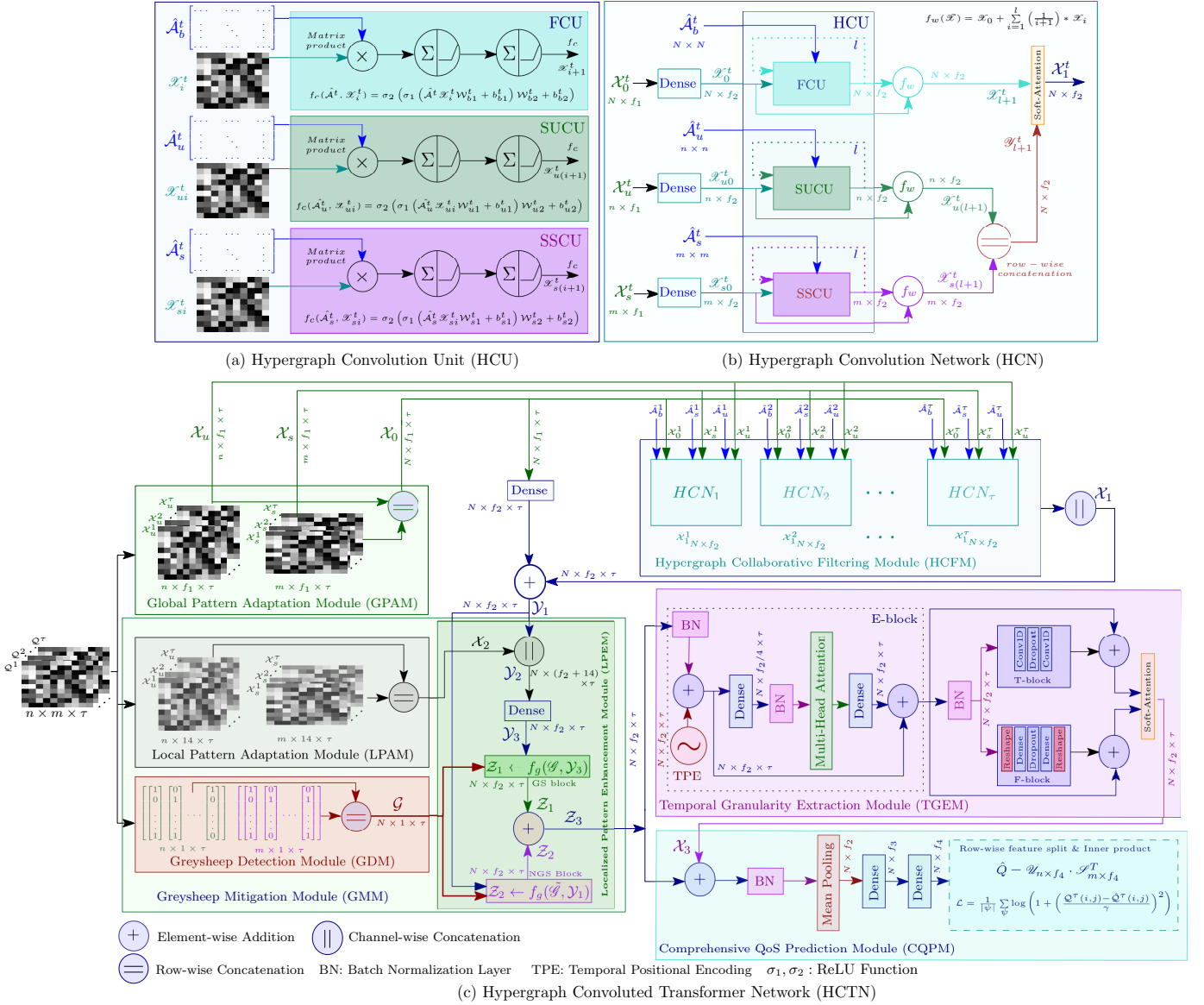


Fig. 2: The architecture of HCTN: (a) Hypergraph Convolution Unit (HCU), (b) Hypergraph Convolution Network (HCN), (c) End-to-end architecture of Hypergraph Convolved Transformer Network (HCTN) for real-time temporal QoS prediction

(b) *Second-order User Interaction Graph (SUIG)*: The SUIG, denoted by $\mathcal{G}_u^t = (\mathcal{V}_u, \mathcal{E}_u^t)$, represents the relationship between two users. An edge $(v_i^u, v_j^u) \in \mathcal{E}_u^t$ exists if the users corresponding to v_i^u and v_j^u both invoked at least one common service at t , i.e., $\exists s_k \in \mathcal{S}$, such that $\mathcal{Q}(i, k, t) \neq 0$ and $\mathcal{Q}(j, k, t) \neq 0$, which means, $\exists v_k^s \in \mathcal{V}_s$, such that $\{v_i^u, v_k^s, v_j^u\} \in \mathcal{E}^t$.

(c) *Second-order Service Interaction Graph (SSIG)*: The SSIG, denoted by $\mathcal{G}_s^t = (\mathcal{V}_s, \mathcal{E}_s^t)$, represents the relationship between two services. An edge $(v_i^s, v_j^s) \in \mathcal{E}_s^t$ exists if the services corresponding to v_i^s and v_j^s both were invoked by at least one common user at t . This means $\exists u_k \in \mathcal{U}$ such that $\mathcal{Q}(k, i, t) \neq 0$ and $\mathcal{Q}(k, j, t) \neq 0$, indicating that $\{v_i^s, v_k^u, v_j^s\} \in \mathcal{E}^t$ for some $\exists v_k^u \in \mathcal{V}_u$.

An example of these three decomposed graphs from the QIHG is illustrated in Fig. 1.

2) *Hypergraph Convolution Units (HCU)*: We now explain the process of extracting higher-order collaborative features using hypergraph convolution on various graphs, including \mathcal{G}_f^t , \mathcal{G}_u^t , and \mathcal{G}_s^t , each representing distinct relationships. Fig. 2(a) provides an overview of the Hypergraph Convolutional Unit (HCU) architecture. The HCU consists of three convolution units: the First-Order Convolution Unit (FCU), the Second-Order User Convolution Unit (SUCU), and the Second-Order Service Convolution Unit (SSCU). We briefly describe each of them next:

(a) *First-order Convolution Unit (FCU)*: At each time-step t , the FCU operates on the FIG \mathcal{G}_f^t . It takes two inputs: the normalized adjacency matrix $\hat{\mathcal{A}}^t$ of \mathcal{G}_f^t and a pre-processed feature embedding \mathcal{X}_i^t representing all users and services. The FCU then applies graph convolution [26] function f_c to these inputs to extract nonlinear collaborative features, as outlined in the equation presented in Fig. 2(a). The normalized adjacency

matrix $\hat{\mathcal{A}}^t = (\mathcal{D}^t)^{-1/2} \cdot (\mathcal{A}^t + \mathbb{I}) \cdot (\mathcal{D}^t)^{-1/2}$ is obtained using symmetric normalization. The diagonal degree matrix, derived from \mathcal{A}^t , and defined as $\mathcal{D}^t(i, i) = \sum_j \mathcal{A}^t(i, j)$, is used to calculate $\hat{\mathcal{A}}^t$. It is important to note that using $\hat{\mathcal{A}}^t$ helps mitigate numerical instability and sensitivity issues caused by high-degree nodes, unlike when using \mathcal{A}^t directly. Additionally, the identity matrix (\mathbb{I}) is added during normalization to include self-features in the convolution process.

(b) *Second-order User Convolution Unit (SUCU) and Second-order Service Convolution Unit (SSCU)*: At each time-step t , the SUCU and SSCU operate on \mathcal{G}_u^t and \mathcal{G}_s^t , respectively, applying graph convolution functions $f_c(\hat{\mathcal{A}}_u^t, \mathcal{X}_{ui}^t)$ and $f_c(\hat{\mathcal{A}}_s^t, \mathcal{X}_{si}^t)$ to independently extract nonlinear collaborative features $\mathcal{X}_{u(i+1)}^t$ for users and $\mathcal{X}_{s(i+1)}^t$ for services, as shown in the equations in Fig. 2(a).

Here, $\hat{\mathcal{A}}_u^t$ and $\hat{\mathcal{A}}_s^t$ represent the normalized matrices that the SUCU and SSCU receive as input. However, unlike the FCU, which uses adjacency matrices derived from \mathcal{G}_f^t , we instead leverage the incidence matrix \mathcal{H}^t , which is also derived from \mathcal{G}_f^t . This matrix is defined as $\mathcal{H}^t = (h_{ij}^t)_{n \times m} \in \{0, 1\}_{n \times m}$, where $h_{ij}^t = 1$ if $\mathcal{Q}(i, j, t) \neq 0$. The derivation to compute $\hat{\mathcal{A}}_u^t$ and $\hat{\mathcal{A}}_s^t$ is presented in Eq. 1 and Eq. 2.

$$\hat{\mathcal{A}}_u^t = (\mathcal{D}_u^t)^{-1/2} \cdot \mathcal{H}^t \cdot (\mathcal{D}_s^t)^{-1} \cdot (\mathcal{H}^t)^T \cdot (\mathcal{D}_u^t)^{-1/2} \quad (1)$$

$$\hat{\mathcal{A}}_s^t = (\mathcal{D}_s^t)^{-1/2} \cdot (\mathcal{H}^t)^T \cdot (\mathcal{D}_u^t)^{-1} \cdot \mathcal{H}^t \cdot (\mathcal{D}_s^t)^{-1/2} \quad (2)$$

Note that in Eq. 1 and Eq. 2, the degree matrices $(\mathcal{D}_u^t)_{n \times n}$ and $(\mathcal{D}_s^t)_{m \times m}$ are derived from the adjacency matrices \mathcal{A}_u^t and \mathcal{A}_s^t , corresponding to \mathcal{G}_u^t and \mathcal{G}_s^t , respectively. These degree matrices are computed in a similar manner to \mathcal{D}^t .

We now introduce the Hypergraph Convolution Network (HCN), where the HCU serves as the primary component.

3) *Hypergraph Convolution Network (HCN)*: Fig. 2(b) illustrates the overview of the HCN. At each time-step t , the HCN receives the feature embeddings \mathcal{X}_0^t , \mathcal{X}_u^t , and \mathcal{X}_s^t , which are generated by the GPAM module, as inputs. These embeddings are first processed through a dense layer, yielding \mathcal{X}_0^t , \mathcal{X}_{u0}^t , and \mathcal{X}_{s0}^t , which are then fed into the HCU in a loop l times.

To counteract potential information loss caused by the over-smoothing issue commonly encountered with multiple graph convolution layers [27], we aggregate the outputs of each layer using the function $f_w(\mathcal{X}) = \mathcal{X}_0 + \sum_{i=1}^l (1/(i+1)) \mathcal{X}_i$, where $\mathcal{X} = (\mathcal{X}_0, \mathcal{X}_1, \dots, \mathcal{X}_l)$ is a tuple of the convolution outputs of length $(l+1)$. This method balances complexity and feature retention by assigning progressively smaller weights to deeper layer outputs, preserving critical information. Finally, we compute $f_w(\mathcal{X}^t)$, $f_w(\mathcal{X}_u^t)$, and $f_w(\mathcal{X}_s^t)$ to generate \mathcal{X}_{l+1}^t , $\mathcal{X}_{u(l+1)}^t$, and $\mathcal{X}_{s(l+1)}^t$, respectively.

We then aggregate $\mathcal{X}_{u(l+1)}^t$ and $\mathcal{X}_{s(l+1)}^t$ through row-wise concatenation to form \mathcal{X}_{l+1}^t . This concatenated matrix is then combined with \mathcal{X}_{l+1}^t using soft-attention [28] to generate \mathcal{X}_1^t , which represents the refined, enriched collaborative features as the output of the HCN block.

4) *Hypergraph Collaborative Filtering*: We now discuss the working of the HCFM. The HCFM leverages the HCN across the past τ time-steps. For each HCN_t where $1 \leq t \leq \tau$,

the inputs include the normalized matrices $\hat{\mathcal{A}}^t$, $\hat{\mathcal{A}}_u^t$, and $\hat{\mathcal{A}}_s^t$, along with the feature embeddings \mathcal{X}_0^t , \mathcal{X}_u^t , and \mathcal{X}_s^t . The outputs from each HCN block are concatenated channel-wise to produce the final embedding \mathcal{X}_1 of size $N \times f_2 \times \tau$.

It is worth noting that the HCFM leverages higher-order, nonlinear, and complex collaborative features, which help alleviate data sparsity issues by utilizing the additional interactions captured through \mathcal{G}_u^t and \mathcal{G}_s^t , for each t , where $1 \leq t \leq \tau$. However, during the generation of these collaborative features, crucial initial features that are beneficial for cold-start scenarios may not be preserved. To address this, we introduce a skip connection from the GPAM, where \mathcal{X}_0 is resized and added to \mathcal{X}_1 , producing the feature tensor \mathcal{Y}_1 of the same size. This skip connection mitigates the cold-start issue and provides stability in training the HCTN. In the next section, we incorporate the module designed to tackle the greysheep problem.

C. Greysheep Mitigation Module (GMM)

While exploring collaborative features, GPAM and HCFM assume user and service preferences are consistent and QoS data remain reliable with time. However, a few user or service characteristics may not be coherent with others due to their deviant pattern of QoS invocations, referred to as Greysheep [29]. Finding such users (services) and selectively fueling them with their own features obtained from their QoS profiles is essential for robust QoS prediction. In this section, we specifically deal with the greysheep instances whose presence suffers collaborative filtering methods and degrades QoS prediction performance. This module consists of three key components: (a) *Greysheep Detection Module (GDM)*: Identifies greysheep users and services within the given QoS data. (b) *Local Pattern Adaptation Module (LPAM)*: Extracts local features for users and services. (c) *Localized Pattern Enhancement Module (LPEM)*: Injects these local features to address the specific challenges posed by greysheep instances. We first explain the details of the GDM.

1) *Greysheep Detection Module (GDM)*: The primary objective of the GDM is to identify greysheep instances within the dataset. These instances refer to greysheep users (GU) or greysheep services (GS) whose preferences deviate significantly from the norm, resulting in lower QoS prediction performance. Inspired by the approach in [29] for detecting atypical instances, the GDM, as shown in Fig. 2(c), is specifically designed to identify these greysheep instances. Given the QoS invocation tensor $\mathcal{Q}_{n \times m \times \tau}$ for the past τ time-steps, the GDM employs a metric called the Greysheep Discrepancy Index (GDI) to assess each user and service for potential greysheep characteristics.

(a) *Greysheep Discrepancy Index (GDI)*: We adopt the concept introduced in [29] to define the GDI. The GDI of a user u_i (denoted by $\mathbb{G}^t(u_i)$) or a service s_j (denoted by $\mathbb{G}^t(s_j)$) is a scalar value derived by comparing the QoS invocation profile of u_i (i.e., $\mathcal{Q}^t(i, \cdot)$) or of s_j (i.e., $\mathcal{Q}^t(\cdot, j)$) against the overall QoS mean for u_i (represented by $\mu^t(u_i) = \text{mean}(\mathcal{Q}^t(i, \cdot))$) or s_j (represented by $\mu^t(s_j) = \text{mean}(\mathcal{Q}^t(\cdot, j))$). This comparison also takes into account the individual service or user means when u_i interacts with a specific service or when s_j is invoked

by a particular user. Appendix A outlines the detailed GDI calculation. A large GDI value indicates the abnormality of u_i or s_j , guiding the labeling of greysheep users and services.

(b) *Greysheep Labeling*: We define the greysheep indicator tensor \mathcal{G} , with dimensions $N \times 1 \times \tau$, as follows:

$$\mathcal{G}(i, 1, t) = \begin{cases} 1 & \text{if } i \leq n \text{ and } \mathbb{G}^t(u_i) > \mu_{gu}^t + c_1 * \sigma_{gu}^t \\ 1 & \text{if } i > n \text{ and } \mathbb{G}^t(s_i) > \mu_{gs}^t + c_2 * \sigma_{gs}^t \\ 0 & \text{otherwise} \end{cases} \quad (3)$$

where, μ_{gu}^t and σ_{gu}^t represent the mean and standard deviation of the GDI values for users, while μ_{gs}^t and σ_{gs}^t represent the mean and standard deviation of the GDI values for services at time-step t . The positive constants c_1 and c_2 are two tunable hyperparameters. This tensor is then utilized in subsequent operations to obtain fine-tuned features for both users and services. In the next subsection, we introduce our next module, LPAM, which extracts user- and service-specific features that are particularly beneficial for greysheep instances, aiming to enhance prediction accuracy.

2) *Local Pattern Adaptation Module (LPAM)*: The objective of this module is to extract local patterns from the QoS invocation profiles of each user and service. For each time-step t within the τ -time-steps, the LPAM is used to obtain local features for each user $u_i \in \mathcal{U}$ and service $s_j \in \mathcal{S}$ based on their QoS profiles $\mathcal{Q}^t(i, \cdot, t)$ and $\mathcal{Q}^t(\cdot, j, t)$. These local features consist of 14 basic statistical metrics, including minimum, maximum, mean, median, standard deviation, skewness, kurtosis, interquartile range, mean absolute deviation, median absolute deviation, root mean square, absolute energy, entropy, and peak-to-peak difference [30]. These features provide diverse quantitative insights into the central tendencies, variability, and distributions of the data. We store these features in a tensor \mathcal{X}_2 with dimensions $N \times 14 \times \tau$. In this tensor, the first n entries of the first dimension correspond to users, while the remaining m entries correspond to services. We then leverage \mathcal{X}_2 to manage GU and GS. In the next module, we will explain the process of injecting these features into the greysheep instances.

3) *Localized Pattern Enhancement Module (LPEM)*: Since collaborative features alone are insufficient to fully represent the GU and GS, we enhance them with profile-specific features to support representation learning and improve QoS prediction performance. To achieve this, we concatenate the collaborative features, \mathcal{Y}_1 , with profile-specific features, \mathcal{X}_2 , along the second dimension of the tensor, resulting in \mathcal{Y}_2 with dimensions $N \times (f_2 + 14) \times \tau$. \mathcal{Y}_2 is then processed through a fully connected layer to reshape the tensor, generating the output tensor \mathcal{Y}_3 with dimensions $N \times f_2 \times \tau$.

To obtain the embedding for greysheep instances, we introduce a function f_g , as described in Eq. 4, which takes the greysheep indicator tensor \mathcal{G} and \mathcal{Y}_3 to filter out features unique to greysheep instances from regular users and services. This results in the embedding $\mathcal{Z}_1 = f_g(\mathcal{G}, \mathcal{Y}_3)$.

For non-greysheep users and services, indicated by $\tilde{\mathcal{G}} = (\mathbb{1}_{N \times 1 \times \tau} - \mathcal{G})$, only \mathcal{Y}_1 is used, leading to the embedding $\mathcal{Z}_2 = f_g(\tilde{\mathcal{G}}, \mathcal{Y}_1)$. Finally, \mathcal{Z}_1 and \mathcal{Z}_2 are combined to form \mathcal{Z}_3 , which retains the distinguishing features of both greysheep and non-greysheep instances. This \mathcal{Z}_3 is subsequently used in the next module.

$$f_g(\mathcal{G}, \mathcal{Y}) = [\mathcal{Z}^1 \parallel \mathcal{Z}^2 \parallel \dots \parallel \mathcal{Z}^\tau]; \quad \forall t = [1.. \tau], \mathcal{Z}^t = (\mathcal{G}^t e) \odot \mathcal{Y}^t \quad (4)$$

where, e is a $1 \times f_2$ dimensional vector of 1s, \odot denotes the Hadamard product (element-wise multiplication), and \parallel represents channel-wise concatenation.

D. Temporal Granularity Extraction Module (TGEM)

The features obtained from the previous modules are limited in their ability to capture the intricate temporal dynamics necessary for accurate temporal QoS prediction. To address this, we introduce the module TGEM, designed to capture temporal features across different scales. TGEM consists of three primary components: (a) *E-block*: A transformer encoder block [23] that includes multi-head attention mechanisms to capture long-range dependencies. (b) *T-block*: A block dedicated to capturing fine-grained temporal features, which is composed of two 1D convolutional layers for localized temporal feature extraction. (c) *F-block*: A block for extracting fine-grained features at each individual time-step, consisting of two fully connected dense layers. These components, as illustrated in Fig. 2(c), work together to capture temporal features at varying levels of granularity. Each component of TGEM is discussed in detail below:

1) *Temporal Dependency Extractor Block (E-block)*: This block is equipped with a transformer encoder [23], incorporating multi-head attention mechanisms. The E-block applies multiple attention heads in parallel, followed by a fully connected dense layer to capture multiple contexts from the input embedding. Additionally, it incorporates positional encoding to overcome the limitation of multi-head attention in preserving the sequential information of the input data. We adopt sinusoidal positional encoding, similar to [23], to maintain temporal sequence information.

Upon receiving the input \mathcal{Z}_3 from GMM, batch normalization (BN) is applied to re-center and re-scale the features, reducing internal covariate shift and improving training stability and speed [31]. After calculating the temporal positional encoding (TPE) for each user-service feature at each time-step, we add the TPE to $\text{BN}(\mathcal{Z}_3)$ to produce the intermediate result \mathcal{Z}_4 , which is then passed to the multi-head attention block. However, the classical transformer encoder faces scalability challenges with high-dimensional feature embeddings. To address this, rather than passing the combined results directly to the multi-head attention block, we introduce a fully connected dense layer, followed by another batch normalization step. This reduces the dimensionality of the input features by one-fourth, resulting in \mathcal{Z}_5 with dimension $N \times (f_2/4) \times \tau$.

Multi-Head Attention (MHA): \mathcal{Z}_5 contains the features for all users and services across all τ time-steps. For each user or service instance i (out of the N instances), the features across the τ time-steps, denoted as $\mathcal{Z}_5^{[i]}$, are rearranged and concatenated row-wise to form the feature matrix \mathcal{F}_i , with dimensions $\tau \times (f_2/4)$. This matrix is then used as input for the MHA. MHA operates in three steps as follows: First, for each j^{th} head, we generate three different representations of \mathcal{F}_i , namely, the Query $\mathbb{Q}_j = \mathcal{F}_i \mathcal{W}_j^{1[i]}$, the Key $\mathbb{K}_j = \mathcal{F}_i \mathcal{W}_j^{2[i]}$,

and the Value $\mathbb{V}_j = \mathcal{F}_i \mathcal{W}_j^{3[i]}$, where $\mathcal{W}_j^{k[i]}$ (for $k \in 1, 2, 3$) are learnable weights. For simplicity, we refrain from writing bias terms in this representation. In the second step, we compute the scaled-dot product attention using $\mathbb{Q}_j^{[i]}$, $\mathbb{K}_j^{[i]}$, and $\mathbb{V}_j^{[i]}$ for each j^{th} head, as shown in Eq. 5, where d_k represents the dimension of the key used to scale dot-product. It is noted that $\mathbb{H}_j^{[i]}$ accommodates self-attentive output embedding for each head j .

$$\mathbb{H}_j^{[i]}(\mathbb{Q}_j^{[i]}, \mathbb{K}_j^{[i]}, \mathbb{V}_j^{[i]}) = \text{softmax}\left(\frac{(\mathbb{Q}_j^{[i]} \cdot (\mathbb{K}_j^{[i]})^T) / \sqrt{d_k}}{\sqrt{d_k}}\right) \mathbb{V}_j^{[i]} \quad (5)$$

We employ total h_n numbers of heads in E-block. In the third and final step, the output embeddings from all heads are concatenated, followed by a linear transformation to produce the output $\mathcal{Z}_6^{[i]} = MHA(\mathbb{Q}^{[i]}, \mathbb{K}^{[i]}, \mathbb{V}^{[i]}) = (\mathbb{H}_1^{[i]} \parallel \mathbb{H}_2^{[i]} \parallel \dots \parallel \mathbb{H}_{h_n}^{[i]}) \mathcal{W}$; where, \mathcal{W} is learnable weight. Each head captures a specific temporal feature, and their combination captures the different contexts within the input embedding. Finally, $\mathcal{Z}_6^{[i]}$ is reshaped and combined across all user-service instances to form \mathcal{Z}_6 . After the MHA operation, \mathcal{Z}_6 is passed through a dense layer to restore its original dimensions, $N \times f_2 \times \tau$. This restored tensor is then added to \mathcal{Z}_5 using a residual connection, which preserves the collaborative characteristics for users and services, resulting in \mathcal{Z}_7 (as depicted in the E-block of TGEM in Fig. 2(c)). The tensor \mathcal{Z}_7 is then passed through batch normalization, producing \mathcal{Z}_8 , which is subsequently fed into the T-block and F-block. These blocks are explained next to obtain multi-granularity features from \mathcal{Z}_8 .

2) *Fine-Grained Temporal Analyzer Block (T-block)*: To capture fine-grained temporal features, we employ the T-block, which utilizes two 1D convolutional layers (Conv1D) with a dropout layer [32] between them, applied along the temporal dimension of \mathcal{Z}_8 . The first Conv1D layer, with $\tau/4$ filters, performs temporal pooling, reducing the temporal dimension by a factor of four, resulting in an output of $N \times f_2 \times (\tau/4)$. This step ensures that fine-grained features are effectively extracted. The second Conv1D layer, with τ filters, restores the temporal dimension to match that of \mathcal{Z}_8 . Finally, we apply a residual connection by adding \mathcal{Z}_8 to the output, forming the final output \mathcal{Z}_T .

3) *Time-Step Feature Refiner Block (F-block)*: Parallel to the T-block, the F-block is designed to capture coarse-grained features. It employs two fully connected dense layers applied over the feature dimension (i.e., the second dimension of the three-dimensional tensor) of the input, with a dropout layer placed between them. In the F-block, the input tensor \mathcal{Z}_8 is reshaped, interchanging the temporal and feature dimensions. The first dense layer applies a nonlinear transformation that reduces the feature dimension to one-fourth, while the second dense layer restores it to its original dimension through another nonlinear transformation. The output from the second layer is reshaped back and added to \mathcal{Z}_8 via a residual connection from the E-block, resulting in the final output embedding, \mathcal{Z}_F .

Finally, we apply soft-attention over \mathcal{Z}_T and \mathcal{Z}_F to refine the temporal dynamics, yielding \mathcal{X}_3 . It is important to note that while the parallel T-block and F-block enable multi-granularity feature extraction, the E-block captures various meaningful

contexts. The output of the TGEM, \mathcal{X}_3 , is then passed to the comprehensive QoS prediction module for final prediction.

E. Comprehensive QoS Prediction Module (CQPM)

The final module of HCTN is responsible for predicting the QoS of a user-service pair at the τ^{th} time-step. This module combines the feature embeddings \mathcal{Z}_3 from GMM and \mathcal{X}_3 from TGEM through feature addition, followed by batch normalization. Mean-pooling is then applied to average features over the previous τ time-steps. This is followed by two fully connected dense layers. The output of the final dense layer is split row-wise to obtain the features for users and services, with dimensions $\mathcal{U}_{n \times f_4}$ and $\mathcal{S}_{m \times f_4}$, respectively. The QoS value is then computed using the inner product of the user and service features: $\hat{Q}^\tau = \mathcal{U}_{n \times f_4} \cdot \mathcal{S}_{m \times f_4}^T$.

F. Training and Prediction

To address the issue of outliers, we adopt two strategies. First, we adopt the Cauchy loss, denoted by \mathcal{L} , as the training objective. The Cauchy loss, as shown in Eq. 6, is more robust to outliers compared to standard error metrics.

$$\mathcal{L} = \frac{1}{|\psi|} \sum_{\mathcal{Q}^\tau(i,j) \in \psi} \log \left(1 + \left(\left(\mathcal{Q}^\tau(i,j) - \hat{\mathcal{Q}}^\tau(i,j) \right) / \gamma \right)^2 \right) \quad (6)$$

where, ψ represents the set of valid entries in \mathcal{Q}^τ , and γ is a scale hyper-parameter. Second, we apply the unsupervised Isolation Forest algorithm [33] to detect and remove a fixed percentage of outliers, controlled by the hyperparameter λ , highlighting HCTN's performance without outlier interference. AdamW optimizer [34] is used here to train our model.

IV. EXPERIMENTS

In this section, we present our experimental setup and analysis. Our framework was trained offline using TensorFlow 2.16.1 with Python 3.10.13, leveraging an NVIDIA GeForce RTX 4080 GPU. For performance evaluation, the model was tested on a system equipped with an AMD Ryzen-9 7950X 16-core processor and 32 GB RAM.

Datasets: We evaluated our method on two publicly available QoS benchmark datasets from WSDREAM-2 [24] comprising Response Time (RT) and Throughput (TP), denoted by D1 and D2, respectively, which are widely used in recent temporal QoS prediction research [13], [17], [18], [40]–[43]. Detailed statistics of the datasets are provided in Table I.

Train-Test-Validation Partition: Table II details the various training (ψ) and testing (Ω) splits. For each dataset, D1 and

TABLE I. WSDREAM-2 [24] dataset specifications

Dataset Statistics	RT (seconds)	TP (kbps)
# \mathcal{U} , # \mathcal{S} , # \mathcal{T}	142, 4500, 64	142, 4500, 64
# Records, Density	30170567, 73.77%	25652011, 62.72%
Range	0.001 – 19.999	3.65e-5 – 6726.834
Mean, Std. Dev.	3.1773, 6.1279	11.3449, 54.2759

TABLE II. Training-testing splits

Training Density	ψ (%)	5	10	15	20	50
QoS parameters	RT (D1)	D1.1	D1.2	D1.3	D1.4	D1.5
	TP (D2)	D2.1	D2.2	D2.3	D2.4	D2.5

TABLE III. Performance comparison of HCTN with previous methods

Methods	Loss Function	MAE					RMSE				
		D1.1	D1.2	D1.3	D1.4	D1.5	D1.1	D1.2	D1.3	D1.4	D1.5
TF	MSE	2.9184	2.7888	2.500	2.4800	2.2127	4.7508	4.5696	4.4100	4.3900	4.0169
WSPred [6]	MSE	2.5580	2.4990	2.410	2.3000	2.1266	4.3626	4.2892	4.200	4.1500	3.8943
NNCP [35]	MSE	1.8000	1.7500	1.5500	1.5800	1.3000	3.9000	4.0500	3.7500	3.5000	2.9000
BNLFT [36]	MSE	1.2600	1.2400	1.2300	1.2200	1.2000	<u>2.8000</u>	<u>2.5000</u>	<u>2.4800</u>	2.4500	2.4000
AMF [37]	MRE	1.6328	1.5766	1.5527	1.5391	-	-	-	-	-	-
TPMCF [18]	Cauchy	0.9735	0.8132	0.7168	0.6159	0.2528	2.9648	2.6856	2.6191	2.2927	1.5832
HCTN	Cauchy	0.8453	0.6765	0.6133	0.5256	0.2237	2.4486	2.2336	2.1074	1.9754	1.2853
\mathcal{I} (%)		13.17%	16.81%	14.44%	14.66%	11.51%	12.55%	10.66%	15.02%	13.84%	18.82%
Methods	Loss Function	MAE					RMSE				
		D2.1	D2.2	D2.3	D2.4	D2.5	D2.1	D2.2	D2.3	D2.4	D2.5
TF	MSE	8.7997	8.5080	8.400	8.350	7.8045	39.5133	39.2792	39.3000	39.2800	38.6964
TPMCF [18]	Cauchy	7.0860	5.7447	4.8590	4.5136	<u>1.4232</u>	40.1241	37.6999	34.7010	30.5240	20.7425
WSPred [6]	MSE	8.2761	8.0131	7.8500	7.6000	6.8000	39.0962	38.6251	38.5000	37.6000	36.5724
NNCP [35]	MSE	5.1000	4.5000	4.2500	4.1000	3.7500	32.5000	32.5000	25.5000	24.5000	23.5000
AMF [37]	MRE	5.0942	4.6984	4.5398	4.4610	-	37.0818	36.0874	35.6750	35.5216	-
BNLFT [36]	MSE	4.2500	4.1000	3.9000	3.7500	3.4000	24.5000	23.4000	21.5000	22.6000	19.9000
HCTN	Cauchy	3.9693	3.5486	3.3071	2.8671	0.7404	23.8219	21.3090	20.8300	18.8000	4.8526
\mathcal{I} (%)		6.60%	13.49%	15.20%	23.54%	47.98%	2.78%	8.94%	3.17%	16.81%	75.61%

The performance of the second-best method is underlined

D2, we create five variations of training densities, labeled as D1.x and D2.x, where x indicates the percentage of training data utilized. Additionally, 20% of the training data is set aside as the validation dataset.

Evaluation Metrics: To quantify the prediction accuracy, the performance of HCTN was evaluated using two widely adopted error metrics: Mean Absolute Error (MAE) and Root Mean Square Error (RMSE) [17]. MAE measures overall prediction accuracy and is robust to outliers, whereas RMSE is more sensitive to outliers and penalizes significant errors more severely, making it useful for assessing model reliability and precision. Lower values of both MAE and RMSE indicate better prediction performance.

A detailed analysis of the dataset is provided in Appendix B. The hyperparameter configurations used in this study are outlined in Appendix C, and information on the comparison methods can be found in Appendix D.

Experimental Analysis: We now present an analysis of the performance of HCTN, starting with a comparison between HCTN and previous temporal QoS prediction methods.

1) *Performance Comparison of HCTN with Past Methods:* Table III displays the performance of HCTN on the D1 and D2 datasets across five different training densities. HCTN significantly outperformed major previous methods in terms of both MAE and RMSE. The overall performance improvement relative to the second-best method, denoted as \mathcal{I} (%), is detailed in Table III. Additionally, the results indicate that the performance of HCTN improved substantially with higher training density.

2) *Performance Comparison of HCTN with Previous Methods After Outlier Removal:* We compared HCTN with seven leading previous methods after removing 10% of outliers (i.e., $\lambda = 10$) from the D1 and D2 datasets at three different training densities, as detailed in Table IV. HCTN consistently achieved the lowest MAE and RMSE, demonstrating its superior predictive accuracy and robustness relative to other methods. This performance is particularly notable in challenging scenarios where QoS data is susceptible to outliers.

3) *Training Time of HCTN:* HCTN was compared with major previous methods in terms of training time, as shown in Fig. 3. HCTN was $2\times$ faster than TASR [21], the second-fastest method among those reported. Compared to TPMCF [18], which achieved the best prediction accuracy among past

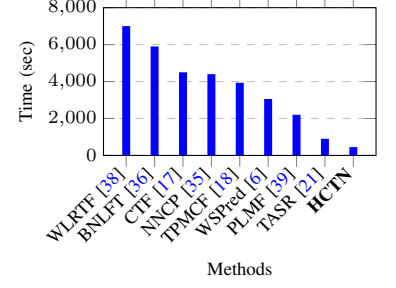


Fig. 3: Training time comparison of HCTN with past methods

TABLE IV. Comparative study of HCTN with $\lambda = 10$

Methods	MAE			RMSE		
	D1.2	D1.4	D1.5	D1.2	D1.4	D1.5
TASR [21]	2.8188	2.7120	2.3292	6.3872	6.1807	5.3942
PLMF [39]	2.6133	2.5932	2.3315	4.5582	4.3536	4.2765
BNLFT [36]	1.0828	1.0575	1.0475	2.6181	2.5809	2.5659
NNCP [35]	1.0796	1.0536	1.0521	2.6401	2.5797	2.5805
WLRTF [38]	1.0560	1.0437	1.0261	2.6009	2.5706	2.5584
CTF [17]	0.9215	0.8981	0.8879	2.5865	2.5579	2.5541
TPMCF [18]	0.4973	0.3864	0.1641	2.2709	1.8885	1.3623
HCTN	0.4713	0.3549	0.1569	1.9017	1.6893	1.1082
\mathcal{I} (%)	5.23%	8.15%	4.39%	16.26%	10.55%	18.65%
Methods	MAE			RMSE		
	D2.2	D2.4	D2.5	D2.2	D2.4	D2.5
TASR [21]	4.3265	3.6419	3.1322	5.9152	5.1844	4.6089
WLRTF [38]	2.9576	2.9568	2.9562	4.9161	4.9160	4.9156
PLMF [39]	2.4712	2.2602	2.3924	3.6705	3.8363	3.8347
NNCP [35]	1.5079	1.4342	1.3926	4.9207	4.7019	4.5026
BNLFT [36]	1.4241	1.3935	1.4319	4.6031	4.4685	4.4319
CTF [17]	1.3567	1.1945	1.0193	3.0436	2.9225	2.7989
TPMCF [18]	1.0101	0.7881	0.2210	2.9564	2.9092	1.4372
HCTN	0.9286	0.7204	0.2187	2.9294	2.8475	1.1385
\mathcal{I} (%)	8.07%	8.59%	1.04%	0.91%	2.12%	20.78%

methods, HCTN was $8.74\times$ faster. This demonstrates that HCTN can be re-trained efficiently with minimal overhead as training density increases, resulting in enhanced prediction performance.

4) *Prediction Time of HCTN:* Real-time systems, especially those involving safety-critical applications, require swift QoS predictions. The average prediction time of HCTN was approximately 2×10^{-6} seconds, a negligible duration compared to the minimum response time of services (0.001 seconds), as indicated in Table I. This demonstrates that our method is well-suited for integration into real-time applications.

5) *Impact of Outliers:* Fig.s 4(a)-(b) depict the performance of HCTN in terms of MAE across varying levels of outlier

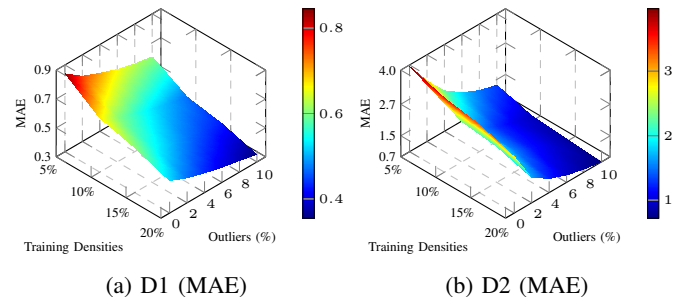


Fig. 4: Impact of outliers on the performance of HCTN

removal ($\lambda = 0$ to $\lambda = 10$, in 2% intervals) on the test datasets corresponding to D1 and D2, with varying training densities. Key observations indicate that as λ increased, more outliers were detected and removed from the test datasets, leading to improved performance of HCTN. However, the rate of improvement gradually decreased across all cases. The initial 2% outlier removal yielded substantial performance gains, with average MAE improvements of 10.53% for the D1 dataset and 34.80% for the D2 dataset. In contrast, the performance gains became less pronounced in the final 2% of outlier removal (from 8% to 10%), with only 4.65% and 14.45% average improvements in MAE for D1 and D2, respectively.

Analysis of the impact of outliers on HCTN performance showed that removing outliers significantly improved predictions, especially in the early stages. However, as more outliers were removed, the rate of improvement slowed, indicating diminishing returns as the data became cleaner. Notably, the most substantial improvements occurred with up to 6% removal, indicating that further removal offered limited additional benefits.

6) *Impact of Greysheep*: HCTN leverages LPAM to extract local features for individual users and services, combining these with the global feature representations from HCFM to effectively manage greysheep instances. Table V shows that HCTN benefits from including local features for greysheep instances as opposed to excluding them (refer to HCTN - GMM in Table V). On average, HCTN achieved a 2.93% and 3.82% improvement over HCTN - GMM on the D1 and D2 datasets, respectively. Furthermore, applying local features to all users and services (refer to HCTN - GDM in Table V) degraded performance. HCTN showed an average improvement of 1.59% and 1.28% over HCTN - GDM on D1 and D2 datasets, respectively. Although these improvements are modest, this is likely due to the small proportion of greysheep users (9.15%) and services (11.51%) identified, as only a limited fraction benefits from the GMM module. Nevertheless, addressing greysheep instances is critical for achieving more robust predictions in challenging cases. This analysis highlights the importance of the greysheep mitigation module (GMM) in selectively integrating local features to enhance prediction accuracy.

Fig.s 5(a)-(b) illustrate the effect of the number of greysheep instances detected by GDM and handled by LPEM, which enhances their feature representation from HCFM by incorporating local patterns of users and services. As the greysheep detection parameters c_1 and c_2 decreased (in Fig.s 5(a)-(b), $c_1 = c_2 = c$), more greysheep instances were identified, resulting in improved HCTN performance. The results show that for $c = 1$, HCTN achieved an average improvement of 4.21% on D1 and 1.34% on D2 compared to $c = 2$. Similarly, the improvement gains for $c = 1$ over $c = 3$ were 5.56% on D1 and 2.29% on D2, suggesting that detecting and incorporating local features for more greysheep instances enhances prediction accuracy.

7) *Module Ablation Study for HCTN*: This analysis justifies the necessity of each module within HCTN by highlighting their contributions to overall performance, measured by MAE, across various λ values on the D1 and D2 datasets. As shown

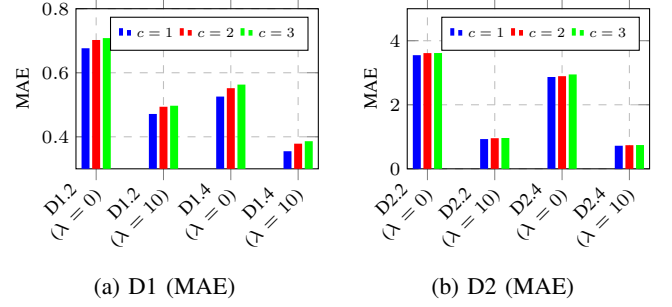


Fig. 5: Impact of greysheep

in Table VI, including HCFM (i.e., HCTN - TGEM) rather than excluding it (i.e., HCTN - HCFM - TGEM) resulted in an average improvement of 2.51% on D1 and 6.11% on D2. Similarly, adding TGEM (i.e., HCTN - HCFM) rather than ablating it (i.e., HCTN - HCFM - TGEM) led to a 1.23% and 2.22% improvement on D1 and D2, respectively. Combining both TGEM and HCFM (i.e., HCTN) yielded even better results, with an average improvement of 1.59% on D1 and 5.44% on D2 over the HCTN - TGEM setup. Furthermore, HCTN showed a notable improvement of 3.73% on D1 and 8.43% on D2 over HCTN - HCFM, highlighting the importance of the HCFM and TGEM modules in optimizing performance.

8) *Feature Ablation Study: Impact of Higher-order Graphs Features*: This analysis highlights the significance of integrating higher-order collaborative features extracted from hypergraphs as defined in this paper. HCFM is designed to extract features from the first-order user-service interaction graph (FIG), as well as from the second-order user interaction graph (SUIG) and second-order service interaction graph (SSIG). FIG captures features from heterogeneous nodes, while SUIG and SSIG focus on homogeneous user-user and service-service node interactions, respectively. Fig. 6 illustrates that combining features from FIG, SUIG, and SSIG yielded superior performance compared to using FIG alone. The combined features resulted in an average improvement of 6.99% on the

TABLE V. Performance (MAE) of HCTN with selectively using LPAM with $c_1 = c_2 = 1$

Datasets	$\lambda = 0$			$\lambda = 10$		
	HCTN - GMM	HCTN - GDM	HCTN	HCTN - GMM	HCTN - GDM	HCTN
D1.2	0.7036	0.6889	0.6765	0.5055	0.4861	0.4713
D1.4	0.5364	0.5330	0.5256	0.3669	0.3617	0.3549
D2.2	3.6713	3.5765	3.5486	0.9550	0.9522	0.9286
D2.4	2.9956	2.9190	2.8671	0.7461	0.7451	0.7204

HCTN - GMM: HCTN without Greysheep Mitigation Module;
HCTN - GDM: HCTN without Greysheep Detection Module, fully utilizing LPAM

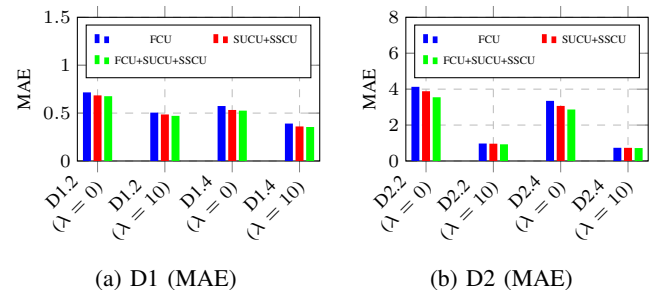


Fig. 6: Ablation study: utilization of hypergraph

TABLE VI. Module ablation study for HCTN (MAE)

Datasets	Modules	λ					
		0	2	4	6	8	10
D1.2	HCTN - HCFM - TGEM	0.7075	0.6335	0.5896	0.5511	0.5223	0.5027
	HCTN - TGEM	0.6995	0.623	0.5803	0.5424	0.5129	0.4925
	HCTN - HCFM	0.7058	0.6299	0.5882	0.5507	0.521	0.5008
	HCTN	0.6765	0.6093	0.5670	0.5298	0.5008	0.4713
	HCTN	0.5559	0.4924	0.4577	0.4267	0.4029	0.3866
D1.4	HCTN - HCFM - TGEM	0.5343	0.4892	0.4536	0.4221	0.3981	0.3814
	HCTN - TGEM	0.5436	0.4798	0.4437	0.4114	0.3869	0.3698
	HCTN - HCFM	0.5256	0.473	0.4373	0.4054	0.3811	0.3549
	HCTN	4.1140	2.3369	1.6610	1.3194	1.1099	0.9642
	HCTN	3.8710	2.3314	1.6557	1.3169	1.1018	0.9550
D2.2	HCTN - HCFM - TGEM	3.9846	2.3325	1.6372	1.3002	1.0904	0.9474
	HCTN - TGEM	3.5486	2.2463	1.6144	1.2820	1.0720	0.9286
	HCTN - HCFM	3.0876	1.7567	1.3180	1.0327	0.8655	0.7562
	HCTN	2.8926	1.7051	1.2810	1.0289	0.8565	0.7476
	HCTN	3.0475	1.7269	1.2865	1.0461	0.8514	0.7446
D2.4	HCTN - HCFM - TGEM	2.8671	1.6767	1.2422	0.9876	0.8288	0.7204
	HCTN - TGEM						
	HCTN - HCFM						
	HCTN						
	HCTN						

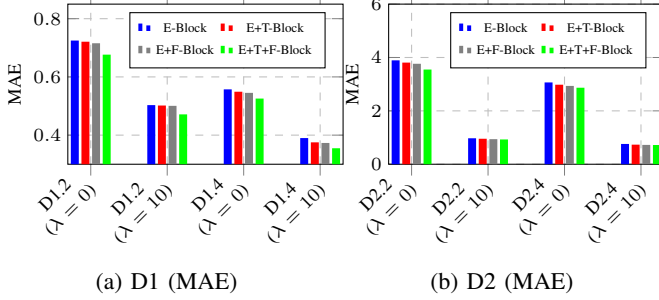


Fig. 7: Ablation study: utilization of various blocks in TGEM

D1 dataset and 19.06% on the D2 dataset over the features extracted from FIG alone. Additionally, the combined features outperformed those extracted from SUIG and SSIG by an average of 1.28% on D1 and 17.88% on D2, highlighting the enhanced value of complex feature integration enabled by the introduction of QIHG.

9) *Feature Ablation Study: Impact of Multi-granularity Temporal Features:* This analysis demonstrates the value of integrating multi-granularity temporal features using TGEM, which includes the E-block, T-block, and F-block. The T-block specializes in capturing fine-grained temporal features, while the F-block focuses on coarse-grained features. Fig. 7 illustrates that combining both fine-grained and coarse-grained features yielded better performance on the D1 and D2 datasets compared to using each feature type individually. The combined features from the E + T + F-blocks provided an average improvement of 6.58% on the D1 dataset and 8.17% on the D2 dataset over the features extracted by the E-block alone. Similarly, E + T + F-blocks resulted in a 5.52% and 5.63% improvement on the D1 and D2 datasets, respectively, compared to the E + T-block setup. Furthermore, E + T + F-blocks outperformed the E + F-block combination by 4.53% on D1 and 4.02% on D2, underscoring the more significant impact of incorporating more comprehensive and diverse feature sets.

10) *Statistical Analysis:* We here present the statistical analysis of the performance of HCTN. Table VII displays the analysis across all datasets, using three different confidence limits (CL): 90%, 95%, and 99%. For example, a CL of 90% indicates that the given samples of QoS values are 90% likely to contain the population's true mean. The confidence interval analysis shows that as the CL increases, the range of the interval broadens, indicating greater certainty about capturing the true mean of QoS values, but with a wider range. This

TABLE VII. Statistical analysis using confidence intervals

CL	D1.2	D1.4	D2.2	D2.4
90%	(0.6812, 0.6904)	(0.5214, 0.5296)	(3.5424, 3.5548)	(2.8166, 2.9176)
95%	(0.6804, 0.6913)	(0.5206, 0.5304)	(3.5412, 3.5560)	(2.8069, 2.9273)
99%	(0.6786, 0.6930)	(0.5191, 0.5320)	(3.5389, 3.5584)	(2.7880, 2.9462)
MAE	0.6765	0.5256	3.5486	2.8671
Std. Dev.	0.0219	0.0207	0.1891	0.1592

reflects a trade-off between precision and confidence in the performance estimates of HCTN.

In summary, HCTN demonstrates superior performance compared to previous methods, with significant improvements in MAE and RMSE across various datasets and training densities. It also excels in handling outliers, provides efficient training and prediction times, and benefits from advanced feature integration, including higher-order graph features and multi-granularity temporal features. A more detailed experimental analysis, including the impact of cold-start and the influence of various hyperparameters on the performance of HCTN, is presented in Appendices E and F.

V. LITERATURE REVIEW

Extensive research has focused on QoS prediction for service composition and recommendations. The classical practices for QoS prediction rely on collaborative filtering (CF), which can be classified into three main types: (a) *Memory-based methods*, which use user-service correlations for prediction [4], [5], [9]; (b) *Model-based methods*, which employ mathematical models to learn parameters for prediction [10], [44]; and (c) *Hybrid methods*, combining memory-based and model-based strategies for improved accuracy [15], [25]. However, most existing methods [4], [5], [9], [10], [25] assume static QoS parameters, neglecting temporal variations. Despite progress, key challenges such as data deficiency, credibility, and learning persist, and we now explore these challenges along with proposed solutions from the literature.

1) *Data Deficiency Problem:* The data deficiency problem in QoS prediction stems from two key factors: (a) sparse user-service interactions, as users cannot evaluate every service, and (b) the cold-start issue, where no historical data exists for new users or services. Approaches based on user-service similarity [13], [21], [42], [45], [46] often struggle with these challenges, leading to inaccurate predictions. CLpred [47] mitigates sparsity through data imputation but struggles with cold-start scenarios. Common strategies like matrix factorization (MF) [18], [37], [39], [41], [44], [48], [49] and tensor factorization (TF) [6], [17], [35], [36], [50]–[56] are often paired with user-service metadata such as geographic or network locations [43], [57], [58]. However, metadata is not always available due to privacy concerns, and MF/TF-based methods often fall short in capturing higher-order QoS features and addressing data credibility issues, leading to compromised prediction accuracy.

2) *Data Credibility Problem:* The data credibility issue is primarily driven by two factors: outliers and greysheep. (a) *Outliers:* These are QoS values significantly deviating from the norm, often due to factors like service status or network workload. Existing methods [13], [14], [21], [39], [40], [42], [45], [46], [48], [49], [57], [59], [60] that do not address outliers typically result in low prediction accuracy. To

mitigate outlier impacts, two main approaches are used: (i) explicit detection using unsupervised methods [33] to exclude outliers, as seen in [17], [18], and (ii) robust loss functions or regularization mechanisms during learning. Techniques like Cauchy loss [17], [18], [50], Huber loss [43], [56], MAE loss [58], and noise contrastive estimation loss [47] offer resilience against outliers. Additionally, regularization methods, including L1, L2, and combinations thereof [6], [35]–[37], [51]–[55], [61], help manage outliers to some extent. (b) *Greysheep*: These are users or services with significantly different QoS patterns that can hinder prediction accuracy and make their QoS values difficult to forecast. Greysheep are often treated as outliers, but they hold unique value within the QoS ecosystem. Existing methods [62]–[64] address greysheep by clustering [62] or reputation-based algorithms [63], [64]. However, these methods may overlook the value of greysheep and may not fully address the challenges they pose.

3) *Data Representation Learning Problem*: The effectiveness of QoS prediction methods largely depends on the chosen data representations, which reveal different aspects of QoS data and explain its variations. Two main types of features are considered: domain-specific features and higher-order non-linear features. (a) *Domain-specific features*: There are primarily two distinct types of domain-specific features. (i) QoS features: Methods like [13], [21], [40], [42], [45], [46] use user-service QoS similarities but often suffer from high sparsity and cold-start issues, leading to low prediction accuracy. Matrix factorization (MF) [37], [48] and tensor factorization (TF) [6], [17], [35], [36], [51], [54], [55] address data deficiency but struggle with capturing higher-order interactions due to their linear nature. (ii) Contextual features: Methods such as [43], [57], [58] use metadata (e.g., IP addresses, geographic locations) to handle cold-start problems effectively, but privacy concerns limit their application. (b) *Higher-order features*: Advanced architectures like Multi-layer Perceptrons (MLPs), Graph Neural Networks (GNNs), and Recurrent Neural Networks (RNNs) (including LSTM and GRU) enhance the ability to capture complex, non-linear, and higher-order features. For instance, [18], [61] utilize GNNs and transformers to model spatial and temporal dependencies. Other methods, such as [13], [39], [41], [43], [47], [49], [56]–[58], combine higher-order features with domain-specific features to improve prediction performance.

In summary, QoS prediction methods often struggle with capturing higher-order interactions, handling non-linearity, addressing cold-start issues, and managing data sparsity. Domain-specific features can be limited by high dimensionality and privacy concerns, while advanced models incorporating higher-order and temporal features may be computationally intensive and may not fully address all data aspects, impacting scalability and accuracy.

In contrast, our approach leverages a Hypergraph Convolutional Transformer Network (HCTN), which integrates domain-specific features with advanced deep-learning techniques. HCTN overcomes traditional limitations by combining non-negative matrix decomposition with robust deep learning architectures, effectively addressing data deficiency, cold-start issues, and credibility problems. It captures complex, non-

linear relationships and higher-order features, improving prediction accuracy and scalability while addressing privacy and dimensionality challenges.

VI. CONCLUSION

This paper addresses the anomaly-resilient real-time temporal QoS prediction problem by introducing HCTN, a Hypergraph Convolutional Transformer Network. HCTN makes three key contributions to improve the prediction performance: (a) For the data deficiency problem caused by sparse QoS interactions and cold-start, we leverage non-negative matrix decomposition, which provides collaborative features to handle the sparsity and cold-start. We further employ the hypergraph collaborative filtering module, which aids with additional connections obtained from hyper-edges to mitigate the high sparsity and exploit the higher-order, nonlinear, and complex features. (b) To handle data credibility issues caused by outliers and greysheep users/services, we apply a robust loss function for training and propose a sparsity-resilient time-aware solution to detect the greysheep, which is then facilitated with their pattern-specific features to alleviate the issue of greysheep. (c) We solve the data representation learning problem by employing domain-specific features using non-negative matrix factorization and incorporating the higher-order complex features by proposing advanced deep learning architectures based on hypergraph convolution and transformer. HCTN consistently outperformed major past methods in prediction performance and training time and is suitable for real-time applications due to negligible prediction time compared to the services' response time. As technology evolves, Machine Learning (ML) services are increasingly crucial for enabling fast, intelligent, and efficient systems. In future work, we aim to investigate energy-efficient ML service selection to enhance prediction accuracy and sustainability.

REFERENCES

- [1] T. Erl, *Service-oriented architecture: a field guide to integrating XML and web services*. Prentice Hall PTR, 2004.
- [2] Y. Duan *et al.*, "Everything as a Service (XaaS) on the Cloud: Origins, Current and Future Trends," in *ICCC*, 2015, pp. 621–628.
- [3] N. Knyazev *et al.*, "The bandwagon effect: Not just another bias," in *ACM SIGIR, ICTIR*, 2022, p. 243–253.
- [4] J. S. Breese *et al.*, "Empirical Analysis of Predictive Algorithms for Collaborative Filtering," in *UAI*, 1998, p. 43–52.
- [5] B. Sarwar *et al.*, "Item-Based Collaborative Filtering Recommendation Algorithms," in *ACM WWW*, 2001, p. 285–295.
- [6] Y. Zhang *et al.*, "WSPred: A Time-Aware Personalized QoS Prediction Framework for Web Services," in *IEEE ISSRE*, 2011, pp. 210–219.
- [7] S. H. Ghafouri *et al.*, "A Survey on Web Service QoS Prediction Methods," *IEEE TSC*, vol. 15, no. 4, pp. 2439–2454, 2022.
- [8] Z. Zheng *et al.*, "Web Service QoS Prediction via Collaborative Filtering: A Survey," *IEEE TSC*, vol. 15, no. 4, pp. 2455–2472, 2022.
- [9] —, "QoS-Aware Web Service Recommendation by Collaborative Filtering," *IEEE TSC*, vol. 4, no. 2, pp. 140–152, 2011.
- [10] D. D. Lee *et al.*, "Learning the parts of objects by non-negative matrix factorization," *Nature*, vol. 401, pp. 788–791, 1999.
- [11] Z. Zheng *et al.*, "Collaborative Web Service QoS Prediction via Neighborhood Integrated Matrix Factorization," *IEEE TSC*, vol. 6, no. 3, pp. 289–299, 2013.
- [12] Y. Wu *et al.*, "An Embedding Based Factorization Machine Approach for Web Service QoS Prediction," in *Service-Oriented Computing*. Springer, 2017, pp. 272–286.
- [13] G. Zou *et al.*, "DeepTSQP: Temporal-Aware Service QoS Prediction via Deep Neural Network and Feature Integration," *Know.-Based Syst.*, vol. 241, no. C, 2022.

- [14] T. Liang *et al.*, “Recurrent Neural Network Based Collaborative Filtering for QoS Prediction in IoV,” *IEEE TITS*, vol. 23: 3, pp. 2400–2410, 2022.
- [15] S. Chattopadhyay *et al.*, “OffDQ: An Offline Deep Learning Framework for QoS Prediction,” in *The ACM Web Conf. 2022*, p. 1987–1996.
- [16] Z. Wang *et al.*, “HSA-Net: Hidden-State-Aware Networks for High-Precision QoS Prediction,” *IEEE TPDS*, vol. 33: 6, pp. 1421–1435, 2022.
- [17] F. Ye *et al.*, “Outlier-Resilient Web Service QoS Prediction,” in *The Web Conf.*, 2021, p. 3099–3110.
- [18] S. Kumar *et al.*, “TPMCF: Temporal QoS Prediction Using Multi-Source Collaborative Features,” *IEEE TNSM*, vol. 21: 4, pp. 3945–3955, 2024.
- [19] J. Zhu *et al.*, “BGCL: Bi-subgraph network based on graph contrastive learning for cold-start QoS prediction,” *KBS*, vol. 263, 2023.
- [20] M. Liu *et al.*, “QoSGNN: Boosting QoS Prediction Performance With Graph Neural Networks,” *IEEE TSC*, vol. 17, no. 02, pp. 645–658, 2024.
- [21] S. Ding *et al.*, “Time-Aware Cloud Service Recommendation Using Similarity-Enhanced Collaborative Filtering and ARIMA Model,” *Decis. Support Syst.*, vol. 107, p. 103–115, 2018.
- [22] S. Hu *et al.*, “Temporal-Aware QoS Prediction via Dynamic Graph Neural Collaborative Learning,” in *ICSOC*, 2022, pp. 125–133.
- [23] A. Vaswani *et al.*, “Attention is All You Need,” in *NIPS*, 2017, p. 6000–6010.
- [24] Z. Zheng *et al.*, “Investigating QoS of Real-World Web Services,” *IEEE TSC*, vol. 7, no. 1, pp. 32–39, 2014.
- [25] S. Kumar *et al.*, “TRQP: Trust-Aware Real-Time QoS Prediction Framework Using Graph-Based Learning,” in *ICSOC*, 2022, pp. 143–152.
- [26] T. N. Kipf and M. Welling, “Semi-Supervised Classification with Graph Convolutional Networks,” in *ICLR*, 2017.
- [27] Z. Wu *et al.*, “A Comprehensive Survey on Graph Neural Networks,” *IEEE TNNLS*, vol. 32, no. 1, pp. 4–24, 2021.
- [28] K. Xu *et al.*, “Show, attend and tell: Neural image caption generation with visual attention,” in *ICML*, vol. 37, 2015, pp. 2048–2057.
- [29] B. Gras *et al.*, “Identifying Grey Sheep Users in Collaborative Filtering: A Distribution-Based Technique,” in *UMAP*. ACM, 2016, p. 17–26.
- [30] M. Barandas *et al.*, “TSFEL: Time Series Feature Extraction Library,” *SoftwareX*, vol. 11, p. 100456, 2020.
- [31] S. Ioffe *et al.*, “Batch normalization: accelerating deep network training by reducing internal covariate shift,” ser. ICML, 2015, p. 448–456.
- [32] N. Srivastava *et al.*, “Dropout: a simple way to prevent neural networks from overfitting,” *JMLR*, vol. 15, no. 1, pp. 1929–1958, 2014.
- [33] F. T. Liu *et al.*, “Isolation-Based Anomaly Detection,” *ACM TKDD*, vol. 6, no. 1, 2012.
- [34] I. Loshchilov *et al.*, “Decoupled Weight Decay Regularization,” in *ICLR*, 2019.
- [35] W. Zhang *et al.*, “Temporal QoS-Aware Web Service Recommendation via Non-Negative Tensor Factorization,” in *ACM WWW*, 2014, p. 585–596.
- [36] X. Luo *et al.*, “Temporal Pattern-Aware QoS Prediction via Biased Non-Negative Latent Factorization of Tensors,” *IEEE Trans. on Cybernetics*, vol. 50, no. 5, pp. 1798–1809, 2020.
- [37] J. Zhu *et al.*, “Online QoS Prediction for Runtime Service Adaptation via Adaptive Matrix Factorization,” *IEEE TPDS*, vol. 28, no. 10, pp. 2911–2924, 2017.
- [38] X. Chen *et al.*, “Robust Tensor Factorization with Unknown Noise,” in *IEEE CVPR*, 2016, pp. 5213–5221.
- [39] R. Xiong *et al.*, “Personalized LSTM Based Matrix Factorization for Online QoS Prediction,” in *IEEE ICWS*, 2018, pp. 34–41.
- [40] “A two-dimensional time-aware cloud service recommendation approach with enhanced similarity and trust,” *JPDC*, vol. 190, p. 104889, 2024.
- [41] P. Zhang *et al.*, “Generative-Adversarial-Based Feature Compensation to Predict Quality of Service,” *IEEE TSC*, vol. 17: 1, pp. 209–223, 2024.
- [42] G. Zou *et al.*, “TRCF: Temporal Reinforced Collaborative Filtering for Time-Aware QoS Prediction,” *IEEE TSC*, no. 01, pp. 1–14, 5555.
- [43] J. Zhou *et al.*, “Spatial Context-Aware Time-Series Forecasting for QoS Prediction,” *IEEE TNSM*, vol. 20, no. 2, pp. 918–931, 2023.
- [44] W. Lo *et al.*, “An Extended Matrix Factorization Approach for QoS Prediction in Service Selection,” in *9th IEEE ICSC*, 2012, pp. 162–169.
- [45] E. Tong *et al.*, “A Missing QoS Prediction Approach via Time-Aware Collaborative Filtering,” *IEEE TSC*, vol. 15, no. 6, pp. 3115–3128, 2022.
- [46] E. Jawabreh *et al.*, “Enhanced Time-Aware Collaborative Filtering for QoS Web Service Prediction,” in *ESOCC*, 2023, p. 70–83.
- [47] Y. Yin *et al.*, “Time-Aware Smart City Services Based on QoS Prediction: A Contrastive Learning Approach,” *IEEE IIOT*, vol. 10, no. 21, pp. 18 745–18 753, 2023.
- [48] S. Li *et al.*, “Time-Aware QoS Prediction for Cloud Service Recommendation Based on Matrix Factorization,” *IEEE Access*, vol. 6, pp. 77 716–77 724, 2018.
- [49] M. Wang *et al.*, “MF-Informer for long-term QoS prediction in edge-cloud collaboration environments,” *Wireless Networks*, pp. 1–16, 2024.
- [50] J. Mi *et al.*, “RNL: A Robust and Highly-Efficient Model for Time-Aware Web Service QoS Prediction,” in *ICIC*, 2023, p. 27–39.
- [51] P. Tang *et al.*, “Temporal pattern-aware QoS prediction by Biased Non-negative Tucker Factorization of tensors,” *Neurocomputing*, vol. 582, p. 127447, 2024.
- [52] H. Wu *et al.*, “Advancing Non-Negative Latent Factorization of Tensors With Diversified Regularization Schemes,” *IEEE TSC*, vol. 15, no. 3, pp. 1334–1344, 2022.
- [53] X. Luo *et al.*, “Adjusting Learning Depth in Nonnegative Latent Factorization of Tensors for Accurately Modeling Temporal Patterns in Dynamic QoS Data,” *IEEE TASE*, vol. 18, no. 4, pp. 2142–2155, 2021.
- [54] S. Wang *et al.*, “Multi-Dimensional QoS Prediction for Service Recommendations,” *IEEE TSC*, vol. 12, no. 1, pp. 47–57, 2019.
- [55] H. Wu and X. Luo, “Instance-Frequency-Weighted Regularized, Non-negative and Adaptive Latent Factorization of Tensors for Dynamic QoS Analysis,” in *ICWS*, 2021, pp. 560–568.
- [56] Y. Zhang *et al.*, “Recurrent Tensor Factorization for Time-Aware Service Recommendation,” *Appl. Soft Comput.*, vol. 85, no. C, 2019.
- [57] M. Wang *et al.*, “A Location-Based Approach for Web Service QoS Prediction via Multivariate Time Series Forecast,” in *IEEE ICSESS*, 2020, pp. 36–39.
- [58] B. Li *et al.*, “QoS Prediction Based on Temporal Information and Request Context,” *SOCA*, vol. 15, no. 3, p. 231–244, 2021.
- [59] X. Fan *et al.*, “CASR-TSE: Context-Aware Web Services Recommendation for Modeling Weighted Temporal-Spatial Effectiveness,” *IEEE TSC*, vol. 14, no. 1, pp. 58–70, 2021.
- [60] C. Wu *et al.*, “Time-Aware and Sparsity-Tolerant QoS Prediction Based on Collaborative Filtering,” in *IEEE ICWS*, 2016, pp. 637–640.
- [61] S. Hu *et al.*, “Temporal-Aware QoS Prediction via Dynamic Graph Neural Collaborative Learning,” in *ICSOC*, 2022, p. 125–133.
- [62] C. Wu *et al.*, “QoS Prediction of Web Services Based on Two-Phase K-Means Clustering,” in *IEEE ICWS*, 2015, pp. 161–168.
- [63] W. Qiu *et al.*, “Reputation-aware QoS value prediction of web services,” in *IEEE SCC*, 2013, pp. 41–48.
- [64] K. Su *et al.*, “TAP: A personalized trust-aware QoS prediction approach for web service recommendation,” *KBS*, vol. 115, pp. 55–65, 2017.

APPENDIX A GREYSHEEP DISCREPANCY INDEX (GDI)

As outlined in Section III.C.1 of the main paper, the primary goal of introducing GDI is to determine how a user or service may exhibit unique characteristics that deviate from the general norms of other users and services. The GDI for a user u_i (denoted as $\mathbb{G}^t(u_i)$) or a service s_j (denoted as $\mathbb{G}^t(s_j)$) at time-step t is a scalar value calculated by comparing the QoS invocation profile of u_i (i.e., $\mathcal{Q}^t(i, \cdot)$) or s_j (i.e., $\mathcal{Q}^t(\cdot, j)$) with the overall QoS mean for u_i (denoted as $\mu^t(u_i) = \text{mean}(\mathcal{Q}^t(i, \cdot))$) or s_j (denoted as $\mu^t(s_j) = \text{mean}(\mathcal{Q}^t(\cdot, j))$). This comparison incorporates individual means for each service when u_i interacts with a service, or for each user when s_j is invoked by a user. The mathematical definitions of $\mathbb{G}^t(u_i)$ and $\mathbb{G}^t(s_j)$ are provided in Eqs. 7 and 8, respectively.

$$\mathbb{G}^t(u_i) = \frac{\sum_{s_j \in \mathcal{S}_i^t} (|\mathcal{Q}^t(i, j) - \mu^t(u_i) - \bar{\mu}^t(s_j)| \times \hat{\mathcal{N}}^t(s_j))}{|\mathcal{S}_i^t|} \quad (7)$$

$$\mathbb{G}^t(s_j) = \frac{\sum_{u_i \in \mathcal{U}_j^t} (|\mathcal{Q}^t(i, j) - \mu^t(s_j) - \bar{\mu}^t(u_i)| \times \hat{\mathcal{N}}^t(u_i))}{|\mathcal{U}_j^t|} \quad (8)$$

where, \mathcal{S}_i^t represents the set of services invoked by u_i at time-step t , and \mathcal{U}_j^t represents the set of users that invoked service

s_j at t . The mean-centered QoS values for u_i and s_j , denoted by $\bar{\mu}^t(s_j)$ and $\bar{\mu}^t(u_i)$ respectively, are defined as follows:

$$\bar{\mu}^t(s_j) = \frac{\sum_{u_i \in \mathcal{U}_j^t} \left(\mathcal{Q}^t(i, j) - \max_{u_i \in \mathcal{U}_j^t} \mathcal{Q}^t(i, j) - \min_{u_i \in \mathcal{U}_j^t} \mathcal{Q}^t(i, j) \right)}{|\mathcal{U}_j^t| - 2} \quad (9)$$

$$\bar{\mu}^t(u_i) = \frac{\sum_{s_j \in \mathcal{S}_i^t} \left(\mathcal{Q}^t(i, j) - \max_{s_j \in \mathcal{S}_i^t} \mathcal{Q}^t(i, j) - \min_{s_j \in \mathcal{S}_i^t} \mathcal{Q}^t(i, j) \right)}{|\mathcal{S}_i^t| - 2} \quad (10)$$

Additionally, $\hat{\mathcal{N}}^t(u_i)$ and $\hat{\mathcal{N}}^t(s_j)$ represent the normalized standard deviation for u_i and s_j at time-step t , as shown in Eq. 11 and Eq. 12, respectively.

$$\hat{\mathcal{N}}^t(u_i) = 1 - \left(\frac{\sigma^t(u_i) - \min_{u_k \in \mathcal{U}} \sigma^t(u_k)}{\max_{u_k \in \mathcal{U}} \sigma^t(u_k) - \min_{u_k \in \mathcal{U}} \sigma^t(u_k)} \right) \quad (11)$$

$$\hat{\mathcal{N}}^t(s_j) = 1 - \left(\frac{\sigma^t(s_j) - \min_{s_k \in \mathcal{S}} \sigma^t(s_k)}{\max_{s_k \in \mathcal{S}} \sigma^t(s_k) - \min_{s_k \in \mathcal{S}} \sigma^t(s_k)} \right) \quad (12)$$

where, $\sigma^t(u_i) = sd(\mathcal{Q}^t(i, \cdot))$ and $\sigma^t(s_j) = sd(\mathcal{Q}^t(\cdot, j))$ represent the standard deviation of the QoS vectors corresponding to u_i and s_j at time-step t , respectively.

A high value of $\hat{\mathcal{N}}^t(u_i)$ or $\hat{\mathcal{N}}^t(s_j)$ generally indicates a consistent QoS invocation pattern for u_i or s_j at time-step t . Therefore, when calculating the GDI of a user u_i in relation to its individual service invocation s_j , we use $\hat{\mathcal{N}}^t(s_j)$ as a weight. This weight reflects the consistency of s_j and helps to determine whether an abnormal value is attributable to u_i or s_j . Similarly, the GDI for s_j is calculated. A high GDI value for u_i or s_j indicates a significant abnormality. Based on these GDI values, we labeled the greysheep users and services in the main paper.

APPENDIX B DATASETS

In this section, we provide more information about the datasets utilized in our experiments. We leverage two large-scale QoS datasets from the publicly available WSDREAM-2 [24] repository, namely, Response Time (RT) and Throughput (TP). These datasets capture QoS interactions for 142 users across 4500 web services over 64 time-steps, with a 15-minute interval between each time-step. These datasets are commonly used for time-aware QoS prediction [13], [14], [18], [41], [45], [56]. We now discuss the characteristics of the datasets.

(i) *Dataset challenges*: In real-life scenarios, a user invokes very few services, eventually leading to situations where a large percentage of QoS data is unknown at a particular time slice, which causes high sparsity in the QoS log matrices. The sparsity is further increased when new users or services, often called cold-start, are added to the QoS ecosystem. The unknown QoS values and cold-start turn out to be data deficiency issues. The datasets further may have the issue of data credibility where the data itself is unreliable due to the presence of outliers and greysheep (GS). The actual cause of generating outliers, however, is unknown, but it is led by

network loads and service status. Moreover, the greysheep is known for its pattern of QoS invocation, which differentiates them from other users or services. Here, we exemplify the concept of GS using a subset of the RT dataset [24]. Fig. B.1 depicts an instance of a GS user compared to three other non-GS users across twelve services based on their response time values. Notably, the QoS pattern of GS1 significantly diverges from non-GS users: 1, 2, and 3. The presence of such users in the QoS logs complicates the feature extraction process and leads to low QoS prediction performance in CF. Therefore, handling such issues is essentially required for high-prediction accuracy.

(ii) *Dataset distribution*: As reported in Section IV of the main paper, the values in the RT and TP datasets range from 0.001 to 19.999 and 3.6534e-5 to 6726.8335, respectively. Table B.1 provides further details on the distribution of both datasets. Notably, both datasets are positively skewed, with most QoS values concentrated on the left side of the distribution. This skew complicates the interpretation of complex features, necessitating non-linear models to capture the underlying patterns, which is the focus of this paper.

APPENDIX C CONFIGURATION OF HYPERPARAMETERS

Table C.1 details the hyperparameters used for experimental analysis in the main manuscript. We aim to optimize model performance across various configurations by systematically adjusting these hyperparameters. We further provide a detailed experimental study of these parameters in Appendix F.

APPENDIX D COMPARISON METHODS

The experiments in the main manuscript are compared with the following representative methods:

- (i) TF: This is a simple tensor factorization (TF) implementation to exploit the triadic relationship among user, service and time.
- (ii) WSPred [6]: Besides TF, this paper leveraged the average QoS value constraints for personalized QoS prediction.
- (iii) NNCP [35]: This paper introduced a non-negative TF using the canonical polyadic decomposition. The user, service and time latent factors are then approximated using the multiplicative updating (MU) algorithm.

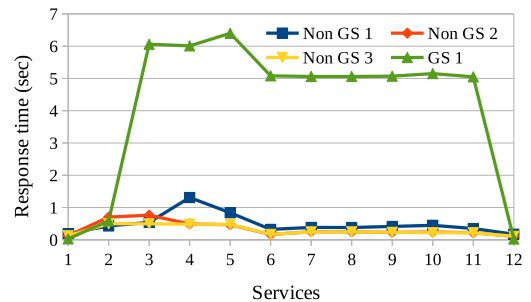


Fig. B.1: Example of a greysheep user

TABLE B.1. Range-wise analysis of QoS datasets

RT (seconds)	Range	0.001 – 0.5	0.5 – 1	1 – 2	2 – 3	3 – 5	5 – 10	10 – 15	15 – 19.999
	Percentage	56.44%	15.55%	8.89%	3.04%	3.51%	4.02%	1.80%	6.75%
TP (kbps)	Range	3.6534e-5 – 25	25 – 50	50 – 100	100 – 250	250 – 500	500 – 1000	1000 – 2500	2500 – 6726.8335
	Percentage	90.66%	3.81%	2.57%	1.97%	0.69%	0.26%	0.0378%	0.0008%

TABLE C.1. Parameter settings of HCTN

Parameters	Description	Values
τ	Time Window	{2, 4, 6, 8, 10, 12, 14}
l	HCN layers	{1, 2, 3, 4}
h_n	No. of heads	{1, 2, 3, 4, 5}
d_k	Head size	{32, 64, 128, 256, 512}

(iv) BNLFT [36]: This method introduced linear biases to non-negative TF, incorporating the MU scheme and an alternating direction method for faster convergence.

(v) WLRTF [38]: This paper proposed a weighted low-rank TF to solve reliability and random noise issues in TF methods by modeling them with a mixture of Gaussians, with parameters learned through the expectation-maximization algorithm.

(vi) AMF [37]: This method introduced an online QoS prediction algorithm using adaptive matrix factorization (MF). In each time slice, a new MF model was iteratively trained, leveraging the previously trained model for time-aware QoS prediction.

(vii) TASR [21]: This paper addressed the QoS prediction problem using a two-stage approach: first, a similarity-based collaborative filtering (CF) algorithm was applied to mitigate sparsity, and then the ARIMA model was used to treat QoS prediction as a time series problem.

(viii) PLMF [39]: This method leveraged LSTM and MF to learn the user and service latent factors for a personalized online QoS prediction.

(ix) CTF [17]: This paper proposed an outlier-resilient TF method incorporating the Cauchy loss function.

(x) TPMCF [18]: This method proposed a real-time outlier-resilient approach leveraging a graph convolution network (GCN) and an enhanced transformer encoder to model temporal fluctuations for time-aware QoS prediction.

Positioning of our paper: In this paper, we propose HCTN, an end-to-end anomaly-resilient framework for real-time QoS prediction that utilizes high-order multi-granularity features through a hypergraph convoluted transformer encoder. This approach addresses various challenges, such as data deficiency, data credibility, and data representation in temporal QoS prediction. HCTN effectively mitigates various underlying challenges for highly accurate, time-sensitive QoS prediction, surpassing the limitations of conventional methods.

- Compared to methods (i)-(vi) [6], [35]–[38], which employ TF or adaptive MF to implicitly address sparsity and cold-start issues while exploiting the relationships among users, services, and time slices, these approaches are sensitive to outliers due to their reliance on outlier-sensitive objective functions. Although some methods incorporate regularization terms with the loss function to partially mitigate outlier effects, they avoid handling the greysheep issue, resulting in performance degradation. In contrast, HCTN employs a hypergraph convoluted transformer encoder that uses initial features from MF to address sparsity and cold-

start problems. It leverages local features based on QoS distribution to tackle the greysheep issue and utilizes hypergraph CF through a hypergraph convolution network (HCN) to manage higher-order neighborhood features. The transformer encoder captures temporal relationships and multifaceted information. Finally, the end-to-end model learning of HCTN incorporating the Cauchy loss function to handle outliers, demonstrates superior prediction performance and reduced learning time compared to the existing methods, as evidenced by experiments presented in the main paper.

- TASR [21] uses ARIMA to model time-aware QoS prediction as a time-series problem. However, ARIMA-based methods assume stationary time series and require a data imputation mechanism to address sparse QoS invocation before application. Further, TASR struggles with cold-start issues due to its reliance on sparsity-sensitive imputation and fails to address outliers and greysheep issues. In contrast, HCTN does not make such assumptions and does not require explicit data imputation. Additionally, HCTN employs a transformer encoder to effectively model time-aware characteristics, overcoming the limitations of ARIMA. fails to address outliers and greysheep issues. In contrast,
- PLMF [39] leverages LSTM-based architectures to capture temporal features and incorporates MF to deal with data deficiency. However, LSTM struggles with long-range dependencies. In contrast, HCTN employs a transformer encoder, which effectively models such time-based feature modalities.
- CTF [17] uses the Cauchy loss function with TF to address outliers, but struggles to capture higher-order features and to handle greysheep users. HCTN not only manages outliers but also overcomes the limitations faced by CTF in these areas.
- TPMCF [18] employs multi-source collaborative features, leveraging domain knowledge and higher-order hidden patterns using a combination of GCN and transformer encoder architectures. The GCN framework captures spatial features, while a separate transformer network models the temporal correlations among those spatial features. However, training these two distinct architectures separately increases the number of learnable parameters and prolongs the learning time. Although TPMCF addresses data credibility issues to some extent through a robust loss function that mitigates outliers, it fails to handle the greysheep challenge. In contrast, HCTN utilizes an end-to-end deep architecture, eliminating the need to train separate components and providing a sparsity-resilient solution for managing greysheep.

Table D.1 summarizes the various challenges in temporal QoS prediction and existing solutions, highlighting how HCTN positions itself relative to contemporary methods.

TABLE D.1. Literature survey on temporal QoS prediction

Methods	Techniques	Data Deficiency		Data Credibility		Data Representation	
		Sparsity	Cold-start	Outlier	Greysheep	Domain-specific	Higher-order
[21]	ARIMA	✗	✗	✗	✗	✓	✗
[42], [45], [46]	Temporal Average, Smoothing, Decay	✗	✗	✗	✗	✓	✗
[59]		✓	✓	✗	✗	✓	✗
[40], [60]		✓	✓	✗	✓	✓	✗
[37]	Adaptive MF	✓	✓	✓	✗	✓	✗
[48]		✓	✓	✗	✗	✓	✗
[6], [35], [36]	Tensor Factorization	✓	✓	✓	✗	✓	✗
[50]–[55]		✓	✓	✓	✗	✓	✗
[17]		✓	✓	✓	✗	✓	✗
[57], [39]	Long-Short Term Memory (LSTM)	✓	✓	✗	✗	✓	✓
[58]		✓	✓	✓	✗	✓	✓
[13]	Gated Recurrent Units (GRU)	✗	✗	✗	✗	✓	✓
[41]		✓	✓	✗	✗	✓	✓
[14]		✓	✓	✗	✗	✗	✓
[43], [56]		✓	✓	✓	✗	✓	✓
[47]	Transformer	✓	✓	✓	✗	✓	✓
[49]		✓	✓	✗	✗	✓	✓
[61]	Graph Attention + GRU	✓	✗	✗	✗	✗	✓
[18]	Graph Convolution + Transformer	✓	✓	✓	✗	✓	✓
HCTN	Hypergraph Convolved Transformer	✓	✓	✓	✓	✓	✓

✓: Addressed, ✓: Partially addressed, ✗: Not addressed

APPENDIX E IMPACT OF COLD-START

To show the impact of a cold-start on HCTN, we randomly removed the QoS record of a fixed percentage (ξ) of users/ services to simulate the cold-start situation. Our experiments present three different scenarios corresponding to the cold start generated in the following ways: (a) *Cold-start Users (CU)*: where QoS observations of $\xi\%$ of users were removed, (b) *Cold-start Services (CS)*: where QoS records for $\xi\%$ services were removed, and (c) *Cold-start users and services Both (CB)*: where QoS observations for $\xi\%$ of both users and services were removed. Fig. E.1 shows the results of these scenarios, and our key observations are summarized below:

- (i) As ξ increased from 0 to 20 for all cases, HCTN performance declined. Further, for the same value of ξ , the performance degradation was highest in the CB scenario, followed by CS; with CU showing the least decline possibly due to the impact of service on the QoS value of a user-service pair is more prominent than that of a user.
- (ii) As the training density increased, performance increased for all scenarios – CU, CS, and CB, for the same value of ξ . This suggests that even with cold-starts in QoS logs, the effects can be reduced by increasing training density, supplementing the matrix factorization to generate better latent features to handle cold-start. This justifies the requirements of matrix factorization features.

To show the effectiveness of HCTN in addressing the cold-

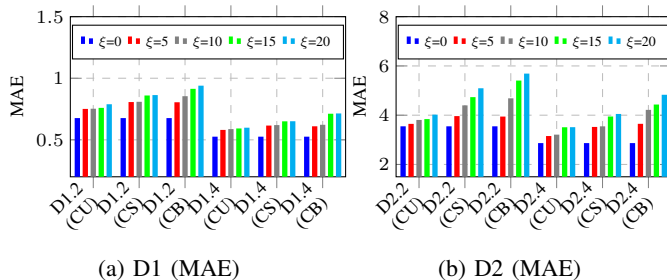


Fig. E.1: Performance of HCTN on cold-start with varying ξ

start problem, we compare it with two prominent past methods, CTF [17] and TPMCF [18], both handle temporal QoS prediction. CTF leverages tensor factorization to handle cold-start situations, while TPMCF uses non-negative matrix factorization to extract user/ service features, helping to alleviate the cold-start issue. Table E.1 presents a comparison of the CB scenario across various cold-start percentages, $\xi = \{0, 5, 10, 15, 20\}\%$, on all datasets. On average, the performance gains of the HCTN over TPMCF on D1 and D2 datasets are 8.01% and 30.01%, respectively, which shows the effectiveness of HCTN over TPMCF. The performance gain of HCTN with respect to CTF is even higher, highlighting the benefits of utilizing higher-order features. This performance boost in HCTN is due to its effective feature utilization in cold-start situations and its ability to model non-linear features.

APPENDIX F IMPACT OF HYPER-PARAMETERS

This section highlights the impact of different hyperparameters on the performance of HCTN.

A. Impact of Time Window

We explore the optimal number of time sequences needed for high QoS prediction performance. Figs F.1(a)-(b) show the experiments by varying the time window (τ) from 2 to 12 with a step size of 2 for all datasets. The performance improves as τ increases for both datasets. At relatively lower τ , performance deteriorates, which is due to not incorporating adequate

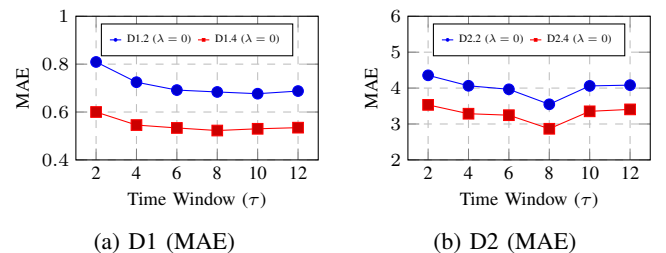
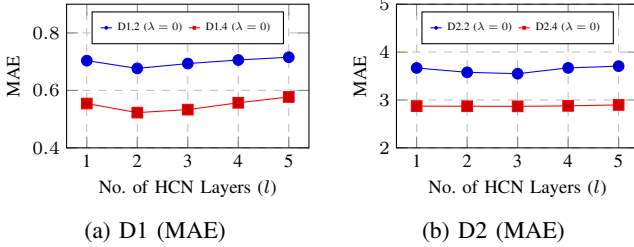


Fig. F.1: Impact of number of time-windows (τ)

TABLE E.1. Cold-start users and service comparison of HCTN with CTF and TPMCF

ξ	D1.2			D1.4			D2.2			D2.4		
	CTF	TPMCF	HCTN	CTF	TPMCF	HCTN	CTF	TPMCF	HCTN	CTF	TPMCF	HCTN
0	1.8908	0.8132	0.6765	1.5337	0.6159	0.5256	10.9274	5.7447	3.5486	8.6924	4.5136	2.8671
5	1.9283	0.8490	0.8050	1.6072	0.6945	0.6099	11.7714	7.0479	3.9443	9.4462	5.4211	3.6499
10	1.9462	0.8993	0.8541	1.6173	0.7069	0.6221	12.7103	7.2463	4.6851	9.9722	5.5479	4.2163
15	1.9538	0.9419	0.9140	1.6235	0.7259	0.7119	12.6588	7.2771	5.4062	10.0847	5.6973	4.4329
20	1.9624	0.9590	0.9397	1.6303	0.7708	0.7142	12.8640	7.3544	5.6886	10.4121	5.9460	4.8293

temporal features essentially required for the high prediction performance. Further, incorporating more time slices enhances QoS prediction up to a certain τ . Specifically, for the D1.2 and D1.4 datasets, we achieved the highest prediction performance for $\tau = 10$ and $\tau = 8$, respectively. Similarly, for D2 datasets, a common $\tau = 10$ achieve the competitive performance. This experiment highlights that while a sufficient number of time slices is crucial for improving model performance by offering more time information, excessively large τ can negatively impact the model.

Fig. F.2: Impact of no. of HCN layers (l)

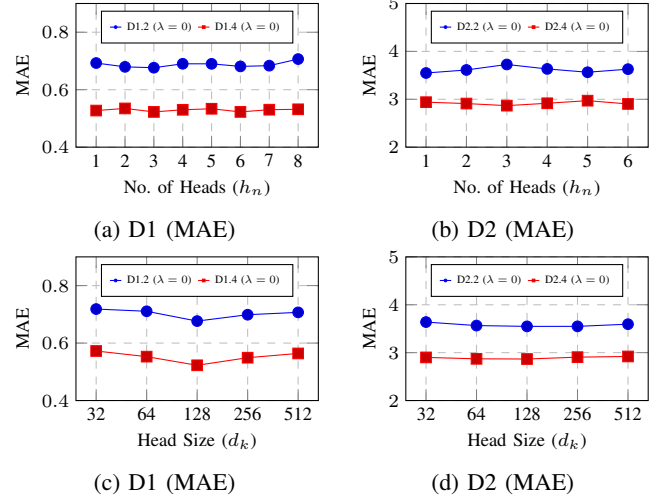
B. Impact of HCN Layers

This experiment shows the utilization of higher-order features obtained using hypergraph collaborative filtering. Fig.s F.2(a)-(b) illustrate the impact of the number of HCN layers (l) by varying from 1 to 5. We achieved competitive performance for $l = 2$ and $l = 3$ for D1 and D2, respectively. However, for higher l , performance deteriorates since, with increased hypergraph convolution layer, the node features propagation may aggregated to give indistinguishable node embedding.

C. Impact of Number of Heads and Head Size in MHA

To optimize the parameters in multi-head attention (MHA), we investigate the sufficient requirements of the number of heads (h_n) and head size (d_k) affecting model performance. Our key observations are as follows.

- (i) Utilizing multiple heads in MHA enables the capture of multi-dimensional information from the features. This experiment intends to find the optimal number of heads that balance prediction performance with the number of learnable parameters, since an increment in the number of heads also increases the learnable parameters. Fig.s F.3(a)-(b) display the impact of h_n for all datasets. We achieved the best performance for $h_n = 3$ and $h_n = 6$ for D1.2 and D1.4, respectively. However, $h_n = 1$ for D2.2, and $h_n = 3$ for D2.4 worked better.
- (ii) The head size refers to the dimensionality of each attention head in MHA. Specifically, it controls the size of features

Fig. F.3: Impact of no. of heads h_n , and head size d_k

each attention head incorporates. For a fixed input features dimension, a smaller head size captures finer details, while larger heads capture broader information. To assess the head size, we vary d_k in powers of 2, ranging from 2^5 to 2^9 . Fig.s F.3(c)-(d) illustrate the performance with different d_k for all datasets. We achieved optimal performance for $d_k = 2^7 = 128$ across all datasets.